European Journal of Medicinal Chemistry 103 (2015) 91–104

Contents lists available at ScienceDirect

European Journal of Medicinal Chemistry

journal homepage: http://www.elsevier.com/locate/ejmech

Research paper

Synthesis, biological evaluation and 3D-QSAR studies of imidazolidine-2,4-dione derivatives as novel protein tyrosine phosphatase 1B inhibitors

Mei-Yan Wang [a, 1], Yuan-Yuan Jin [a, 1], Hui-Yu Wei [b], Li-Song Zhang [a], Su-Xia Sun [a], Xiu-Bo Chen [b], Wei-Li Dong [a], Wei-Ren Xu [c], Xian-Chao Cheng [a, *], Run-Ling Wang [a, **]

[a] Tianjin Key Laboratory on Technologies Enabling Development of Clinical Therapeutics and Diagnostics (Theranostics), School of Pharmacy, Tianjin Medical University, Tianjin 300070, China
[b] Tianjin Medical University Eye Hospital, Tianjin 300384, China
[c] Tianjin Key Laboratory of Molecular Design and Drug Discovery, Tianjin Institute of Pharmaceutical Research, Tianjin 300193, China

ARTICLE INFO

Article history:
Received 4 January 2015
Received in revised form
6 July 2015
Accepted 17 August 2015
Available online 20 August 2015

Keywords:
PTP1B
Imidazolidine-2,4-dione
Synthesis
CoMFA/CoMSIA
Docking

ABSTRACT

Protein tyrosine phosphatase 1B (PTP1B) plays a vital role in the regulation of insulin sensitivity and dephosphorylation of the insulin receptor, so PTP1B inhibitors may be potential agents to treat type 2 diabetes. In this work, a series of novel imidazolidine-2,4-dione derivatives were designed, synthesized and assayed for their PTP1B inhibitory activities. These compounds exhibited potent activities with IC_{50} values at 0.57–172 μM. A 3D-QSAR study using CoMFA and CoMSIA techniques was carried out to explore structure activity relationship of these molecules. The CoMSIA model was more predictive with $q^2 = 0.777$, $r^2 = 0.999$, SEE = 0.013 and $r^2_{pred} = 0.836$, while the CoMFA model gave $q^2 = 0.543$, $r^2 = 0.998$, SEE = 0.029 and $r^2_{pred} = 0.754$. The contour maps derived from the best CoMFA and CoMSIA models combined with docking analysis provided good insights into the structural features relevant to the bioactivity, and could be used in the molecular design of novel imidazolidine-2,4-dione derivatives.

1. Introduction

Type 2 diabetes is associated with a variety of vascular complications resulting from insulin resistance of the human organism [1]. Over 300 million people are now suffering from type 2 diabetes and the incidence of it is still on the rise [2–4]. Therefore, development of specific insulin-sensitizing drugs is pressing.

PTP1B plays as a negative regulator of insulin signaling pathways by dephosphorylating insulin receptor (IR) and IR substrate [5–10]. Studies on PTP1B knockout mice displayed enhanced insulin sensitivity and resistance to high-fat diet induced obesity [11,12], which suggested that PTP1B might be a promising target for type 2 diabetes therapy.

Among all potential inhibitors of PTP1B known so far, ertiprotafib, developed by American Home Products, is the first drug candidate entering PhaseIIclinical trials. Unfortunately, it was withdrawn as a result of undesirable side-effects. Then, ISIS-113715, an antisense inhibitor of the PTP1B gene, is the second one reaching PhaseIIclinical trials [13]. However, despite intensive efforts and great progress [14–24], a safe and efficient PTP1B inhibitor is still a big challenge for medicinal chemists.

During the last decade, glitazones, which shared a common molecular skeleton of 2,4-thiazolidinediones (TZDs), were approved by USA FDA as anti-diabetic drugs. These TZD drugs produced the anti-diabetic effects by agonizing peroxisome proliferator-activated receptor γ. Interestingly, some TZD derivatives also exhibited significant PTP1B inhibitory activities in both experiments performed by Ottana et al. [25,26] and Bhattarai et al. [27]. According to their research, the substituents at N_3 position of TZD scaffold could mimic pTyr group to interact with the receptor [28], and the lipophilic arylidene group at C_5 position of TZD scaffold could improve the stability of receptor-inhibitor binding by hydrophobic interaction. Based on the bioisosteric principle, the TZD scaffold was replaced by imidazolidine-2,4-dione

* Corresponding author.
** Corresponding author.
E-mail addresses: chengxianchao@aliyun.com (X.-C. Cheng), wangrunling@tijmu.edu.cn (R.-L. Wang).
[1] These authors contributed equally to this work.

http://dx.doi.org/10.1016/j.ejmech.2015.08.037
0223-5234/

scaffold, which was then substituted by various benzyl group or alkyl group at N_3 position (R_1), benzyl group at N_1 position (R_2) and para-substituted benzylidene group at C_5 position (R_3) (Fig. 1). These compounds were synthesized and assayed for their PTP1B inhibitory activities, hoping to get similar or better PTP1B inhibitory activities.

Recently, three-dimensional quantitative structure-activity relationship (3D-QSAR) technique has been widely employed to correlate structural descriptors from a cluster of related molecules to their known bioactivity. In terms of PTP1B inhibitors, the 3D-QSAR study of 2-(oxalylamino) benzoic acid analogs [29,30], benzofuran and benzothiophene biphenyls analogs [29], pyridazine analogs [31], and 2,4-thiazolidinedione [32] have been reported. However, the 3D-QSAR research about imidazolidine-2,4-dione derivatives as new PTP1B inhibitors has not been reported till now.

In this paper, the synthesis, biological evaluation and structure activity relationship of novel imidazolidine-2,4-dione derivatives as PTP1B inhibitors were reported. The CoMFA/CoMSIA analysis and docking studies were also performed to investigate compounds-target binding details.

2. Chemistry

The synthetic routes of all the 39 target compounds were shown in Schemes 1–4.

Using 4-hydroxybenzaldehyde and hydantoin as the starting material, compounds **4a**–**e, 5a**–**f** and **6a**–**h** were synthesized via Knoevenagel condensation and alkylation with various halogenated compounds (Scheme 1).

As shown in Scheme 2, N_1-benzyl hydantoin was reacted with methyl bromoacetate using K_2CO_3 as the catalyst to produce **8a**. Compound **8a** was further reacted with 4-hydroxybenzaldehyde to yield compound **9a**. On one hand, **9a** was reacted with halogenated compounds using K_2CO_3 as the catalyst to afford the compounds **10a**–**10c**, which were further hydrolyzed to obtain corresponding **11a**–**11c**. On the other hand, **9a** was directly hydrolyzed to get the target compound **12a**, which was further reacted with halogenated compounds to afford the compounds **13a** and **13b**. In a similar way, the target compounds **9b**, **10d**–**10g**, **11d**–**11f**, **12b** and **13c** were synthesized (Schemes 3 and 4).

3. Results and discussion

3.1. Biological evaluation

Table 1 listed the PTP1B inhibitory activities of the 39 imidazolidine-2,4-dione derivatives. From Table 1, we could clearly see that most of these molecules exhibited mild inhibitory activities against human PTP1B with IC_{50} values at about 0.57–172 μM. Compound **5e** showed the most potent PTP1B inhibitory activity with the IC_{50} value at 0.57 μM.

We can see from Table 1, most molecules were substituted in part R_2 and R_3. However, the most active molecule **5e** ($R_2 = R_3 =$ 2,4-di-Cl-$PhCH_2$) and **10d** ($R_2 = PhCH_2$, $R_3 =$ 4-CH_3OOC-$PhCH_2$) and other molecules with larger hydrophobic aromatic groups in these two positions (**4a**–**4e, 5a, 5c**–**5f, 10a, 10f**–**10g,** and **13a**) appeared to be more active than the ones with relatively small substituents in either of the two places (**6a**–**6c, 6f, 9a, 10b, 11b, 11e, 12a**–**12b,** and **13b**). Besides, some molecules without substituents or with an aryl group in part R_1 exhibited better bioactivities (**4a**–**4e, 5a, 5c**–**5f, 9b, 10a, 10d**–**10g, 13a,** and **13c**). From the above, the conceivable SARs of PTP1B inhibitors observed only from Table 1 is that compounds with hydrophobic, aromatic and bulky substituents in parts R_2 and R_3, and with H or an aromatic group in R_1 would be more likely to acquire higher activities (**4a**–**4e, 5a, 5c**–**5f, 10a, 10d**–**10g,** and **13a**). The hypothesis will be tested in the following 3D-QSAR study.

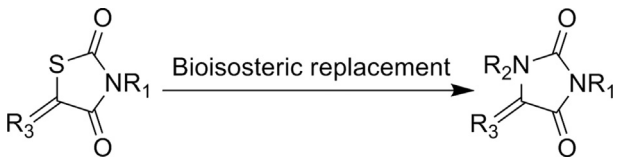

Fig. 1. Design of imidazolidine-2,4-dione derivatives as PTP1B inhibitors.

In this paper, CoMFA/CoMSIA and docking studies were performed to investigate the relationship between biological activities and chemical structures.

3.2. 3D-QSAR analysis

3.2.1. CoMFA/CoMSIA statistical analysis

The CoMFA/CoMSIA models were constructed using 32 imidazolidine-2,4-dione derivatives as the training set. This model was used to predict activities of the test set containing 7 compounds. The statistical data for the best CoMFA/CoMSIA models were summarized in Table 2.

Table 2 showed that the Leave-One-Out (LOO) cross-validated q^2 of the best CoMFA model was 0.543 with 8 optimal components. The q^2 value was correlated to the predictability of the 3D-QSAR model and 0.543 ($q^2 > 0.5$) signified a good predictive ability of the CoMFA model. Non-cross-validated coefficient r^2 of 0.998 with standard error of 0.029 and F value of 277.689 suggested that the linearity of the model was pretty good. The steric field descriptor was 0.427 while the electrostatic descriptor was 0.573, which suggested a greater contribution of electrostatic field than steric field to PTP1B inhibitory activity in CoMFA study.

Table 2 clearly displayed that the best CoMSIA model covered five descriptor fields: steric, electrostatic, hydrophobic, hydrogen-bond donor, and hydrogen-bond acceptor. The relative contribution of the five fields was found to be 0.101 (steric), 0.231 (electrostatic), 0.237 (hydrophobic), 0.225 (hydrogen-bond acceptor) and 0.206 (hydrogen-bond donor), respectively, indicating that compared with steric, the other four fields were more important to biological activity. PLS regression of CoMSIA model showed a q^2 value of 0.777 with 11 optimal components, non-cross-validated r^2 value of 0.999, the standard error of estimate of 0.013 and F value of 344.740. The high q^2 value represented a good predictive ability of the CoMSIA model.

The predictive ability of the CoMFA and CoMSIA models were assessed by the test set of 7 imidazolidine-2,4-dione derivatives, and the results including predicted activities, experimental activities and their residues were listed in Table 3. The predicted pIC_{50} values were in good agreement with the experimental data within a statistically tolerable error range. The predictive correlation coefficient r^2_{pred} was 0.754 and 0.836 for the CoMFA and CoMSIA models, respectively, and the correlations between the predicted values and the experimental values for both models were depicted in Fig. 2.

The above results demonstrated that the constructed 3D-QSAR models were statistically significant and reliable, which could be used to design novel imidazolidine-2,4-dione derivatives with improved PTP1B inhibitory activity.

3.2.2. CoMFA/CoMSIA contour plots

The contour plots of 3D-QSAR analysis were shown in Figs. 3 and 4. The visualization of the results of both CoMFA and CoMSIA models was performed using StDev*Coeff (the standard deviation

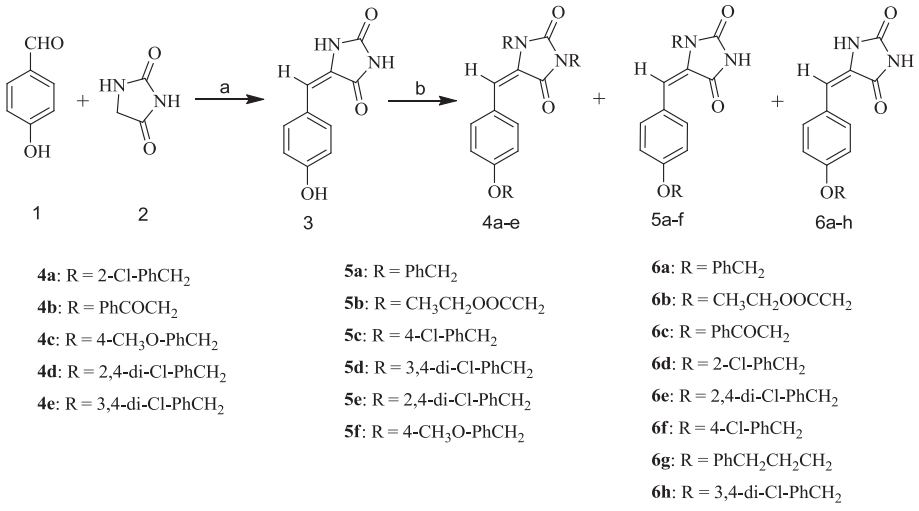

4a: R = 2-Cl-PhCH$_2$
4b: R = PhCOCH$_2$
4c: R = 4-CH$_3$O-PhCH$_2$
4d: R = 2,4-di-Cl-PhCH$_2$
4e: R = 3,4-di-Cl-PhCH$_2$

5a: R = PhCH$_2$
5b: R = CH$_3$CH$_2$OOCCH$_2$
5c: R = 4-Cl-PhCH$_2$
5d: R = 3,4-di-Cl-PhCH$_2$
5e: R = 2,4-di-Cl-PhCH$_2$
5f: R = 4-CH$_3$O-PhCH$_2$

6a: R = PhCH$_2$
6b: R = CH$_3$CH$_2$OOCCH$_2$
6c: R = PhCOCH$_2$
6d: R = 2-Cl-PhCH$_2$
6e: R = 2,4-di-Cl-PhCH$_2$
6f: R = 4-Cl-PhCH$_2$
6g: R = PhCH$_2$CH$_2$CH$_2$
6h: R = 3,4-di-Cl-PhCH$_2$

Scheme 1. Reagents and conditions: (a) piperidine; (b) K_2CO_3, acetone, ethyl bromoacetate or NaH, DMF, organochlorine compounds.

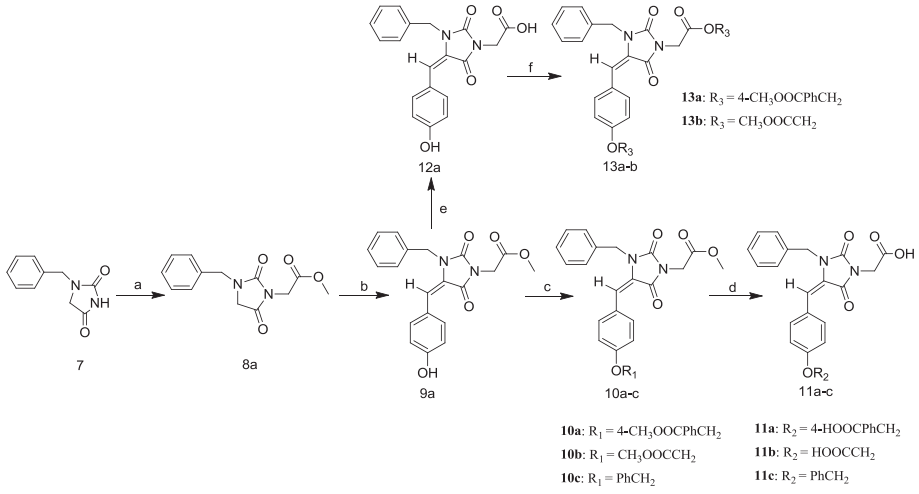

13a: R$_3$ = 4-CH$_3$OOCPhCH$_2$
13b: R$_3$ = CH$_3$OOCCH$_2$

10a: R$_1$ = 4-CH$_3$OOCPhCH$_2$
10b: R$_1$ = CH$_3$OOCCH$_2$
10c: R$_1$ = PhCH$_2$

11a: R$_2$ = 4-HOOCPhCH$_2$
11b: R$_2$ = HOOCCH$_2$
11c: R$_2$ = PhCH$_2$

Scheme 2. Reagents and conditions: (a) K_2CO_3, DMF, methyl bromoacetate; (b) 4-hydroxybenzaldehyde, piperidine, HOAc, toluene; (c) K_2CO_3, DMF, halogenated compounds; (d) Sodium hydroxide solution (1 mol/L), methanol; (e) Sodium hydroxide solution (1 mol/L), methanol; (f) K_2CO_3, DMF/acetone, halogenated compounds.

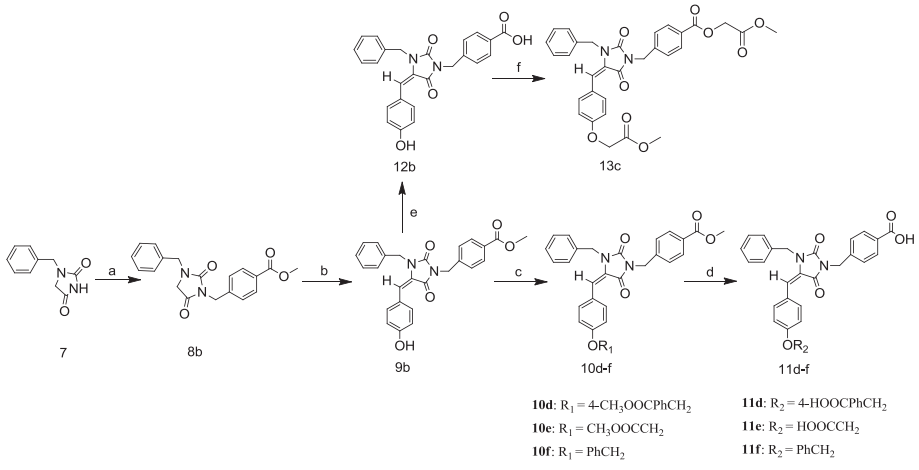

10d: R$_1$ = 4-CH$_3$OOCPhCH$_2$
10e: R$_1$ = CH$_3$OOCCH$_2$
10f: R$_1$ = PhCH$_2$

11d: R$_2$ = 4-HOOCPhCH$_2$
11e: R$_2$ = HOOCCH$_2$
11f: R$_2$ = PhCH$_2$

Scheme 3. Reagents and conditions: (a) K_2CO_3, DMF, methyl 4-(bromomethyl) benzoate; (b) 4-hydroxybenzaldehyde, piperidine, HOAc, toluene; (c) K_2CO_3, DMF, halogenated compounds; (d) Sodium hydroxide solution (1 mol/L), methanol; (e) Sodium hydroxide solution (1 mol/L), methanol; (f) K_2CO_3, DMF, methyl bromoacetate.

and the coefficient) [33,34] mapping option contoured by contribution. Favored and disfavored levels of the contour maps by contribution were set at 80% and 20%, respectively. The most active compound **5e** was embedded into the maps to illustrate its affinity for the steric, electrostatic, hydrophobic, hydrogen-bond acceptor and hydrogen-bond donor regions of inhibitors.

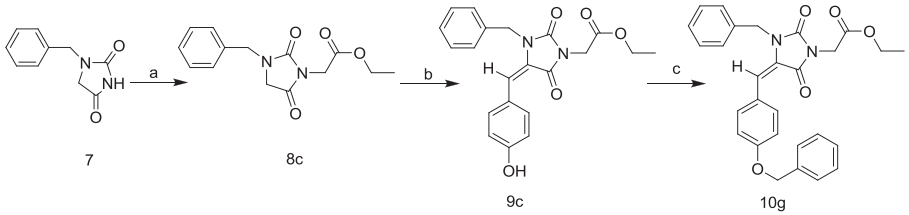

Scheme 4. Reagents and conditions: (a) K_2CO_3, DMF, ethyl 2-bromoacetate; (b) 4-hydroxybenzaldehyde, piperidine, HOAc, toluene; (c) K_2CO_3, DMF, benzyl chloride.

Table 1
Structure and PTP1B inhibitory activities of imidazolidine-2,4-dione derivatives.

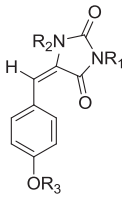

No.	R_1	R_2	R_3	IC_{50} (μM)
4a	2-Cl-$PhCH_2$	2-Cl-$PhCH_2$	2-Cl-$PhCH_2$	3.5
4b	$PhCOCH_2$	$PhCOCH_2$	$PhCOCH_2$	11
4c	4-CH_3O-$PhCH_2$	4-CH_3O-$PhCH_2$	4-CH_3O-$PhCH_2$	7.4
4d	2,4-di-Cl-$PhCH_2$	2,4-di-Cl-$PhCH_2$	2,4-di-Cl-$PhCH_2$	6.6
4e	3,4-di-Cl-$PhCH_2$	3,4-di-Cl-$PhCH_2$	3,4-di-Cl-$PhCH_2$	4.1
5a	H	$PhCH_2$	$PhCH_2$	10
5b	H	$CH_3CH_2OOCCH_2$	$CH_3CH_2OOCCH_2$	133
5c	H	4-Cl-$PhCH_2$	4-Cl-$PhCH_2$	3.3
5d	H	3,4-di-Cl-$PhCH_2$	3,4-di-Cl-$PhCH_2$	1.3
5e	H	2,4-di-Cl-$PhCH_2$	2,4-di-Cl-$PhCH_2$	0.57
5f	H	4-$CH_3O$$PhCH_2$	4-$CH_3O$$PhCH_2$	3.4
6a	H	H	$PhCH_2$	170
6b	H	H	$CH_3CH_2OOCCH_2$	172
6c	H	H	$PhCOCH_2$	155
6d	H	H	2-Cl-$PhCH_2$	15
6e	H	H	2,4-di-Cl-$PhCH_2$	1.7
6f[a]	H	H	4-Cl-$PhCH_2$	122
6g[a]	H	H	$PhCH_2CH_2CH_2$	14
6h	H	H	3,4-di-Cl-$PhCH_2$	11
9a	CH_3OOCCH_2	$PhCH_2$	H	136
9b	4-$CH_3OOCPhCH_2$	$PhCH_2$	H	8.1
10a	CH_3OOCCH_2	$PhCH_2$	4-$CH_3OOCPhCH_2$	6.8
10b	CH_3OOCCH_2	$PhCH_2$	CH_3OOCCH_2	114
10c	CH_3OOCCH_2	$PhCH_2$	$PhCH_2$	110
10d[a]	4-$CH_3OOCPhCH_2$	$PhCH_2$	4-$CH_3OOCPhCH_2$	0.96
10e[a]	4-$CH_3OOCPhCH_2$	$PhCH_2$	CH_3OOCCH_2	9.7
10f	4-$CH_3OOCPhCH_2$	$PhCH_2$	$PhCH_2$	5.1
10g[a]	$CH_3CH_2OOCCH_2$	$PhCH_2$	$PhCH_2$	11
11a	$HOOCCH_2$	$PhCH_2$	4-$HOOCPhCH_2$	103
11b	$HOOCCH_2$	$PhCH_2$	$HOOCCH_2$	122
11c	$HOOCCH_2$	$PhCH_2$	$PhCH_2$	113
11d	4-$HOOCPhCH_2$	$PhCH_2$	4-$HOOCPhCH_2$	89
11e	4-$HOOCPhCH_2$	$PhCH_2$	$HOOCCH_2$	103
11f	4-$HOOCPhCH_2$	$PhCH_2$	$PhCH_2$	96
12a	$HOOCCH_2$	$PhCH_2$	H	142
12b	4-$HOOCPhCH_2$	$PhCH_2$	H	104
13a[a]	4-$CH_3OOCPhCH_2OOCCH_2$	$PhCH_2$	4-$CH_3OOCPhCH_2$	5.4
13b	$CH_3OOCCH_2OOCCH_2$	$PhCH_2$	CH_3OOCCH_2	101
13c[a]	4-$CH_3OOCCH_2OOCPhCH_2$	$PhCH_2$	CH_3OOCCH_2	22

[a] Compounds selected for the test set.

The CoMFA contour plot representing the contribution of steric field was depicted in Fig. 3a. The steric contours were shown in yellow and green, with green regions indicating a steric contribution to activity, while yellow regions indicating a steric hindrance to potency. As shown in Fig. 3a, a large green contour surrounded para-position of the aromatic ring at the C_5 position of the imidazolidine-2,4-dione ring, indicating that increased steric bulk was preferred in the position to improve the activity. This could be confirmed by the fact that compounds containing a bulkier aromatic group at R_3 (**4a**–**4e, 5c**–**5f, 6e, 10a** and **10f**) had higher

Table 2
The PLS statistic results of CoMFA and CoMSIA models.

Statistical Parameters	CoMFA	CoMSIA
Cross-validated (LOO)		
q^2[a]	0.543	0.777
ONC[b]	8	11
Non-cross-validated		
r^2[c]	0.998	0.999
SEE[d]	0.029	0.013
F value[e]	277.689	344.740
r^2_{pred}[f]	0.754	0.836
Field distribution		
Steric	0.427	0.101
Electrostatic	0.573	0.231
Hydrophobic	–	0.237
Hydrogen bond donor	–	0.206
Hydrogen bond acceptor	–	0.171

[a] LOO-cross-validated correlation coefficient.
[b] Optimal components.
[c] Non-cross-validated correlation coefficient.
[d] Standard error of estimate.
[e] F-ratio of F-statistic for the analysis.
[f] Predictive correlation coefficient.

Table 3
Experimental versus predicted activities of training and test set molecules according to the CoMFA and CoMSIA models.

No.	Experimental activity (pIC_{50})	CoMFA		CoMSIA	
		Predict	Residue	Predict	Residue
4a	−0.539	−0.517	−0.022	−0.529	−0.010
4b	−1.045	−1.047	0.002	−1.055	0.010
4c	−0.872	−0.871	−0.001	−0.869	−0.003
4d	−0.820	−0.835	0.015	−0.829	0.009
4e	−0.614	−0.630	0.016	−0.613	−0.001
5a	−1.006	−1.056	0.050	−1.017	0.011
5b	−2.123	−2.099	−0.024	−2.114	−0.009
5c	−0.520	−0.519	−0.001	−0.512	−0.008
5d	−0.127	−0.141	0.014	−0.138	0.011
5e	0.244	0.294	−0.050	0.255	−0.011
5f	−0.528	−0.510	−0.018	−0.539	0.011
6a	−2.230	−2.214	−0.016	−2.232	0.002
6b	−2.236	−2.223	−0.013	−2.244	0.008
6c	−2.191	−2.174	−0.017	−2.190	−0.001
6d	−1.182	−1.179	−0.003	−1.149	−0.033
6e	−0.218	−0.265	0.047	−0.242	0.024
6f[a]	−2.085	−2.117	0.032	−2.076	−0.009
6g[a]	−1.145	−1.612	0.467	−1.505	0.360
6h	−1.042	−1.038	−0.004	−1.040	−0.002
9a	−2.135	−2.165	0.030	−2.148	0.013
9b	−0.911	−0.917	0.006	−0.911	0.000
10a	−0.833	−0.835	0.002	−0.822	−0.011
10b	−2.057	−2.042	−0.015	−2.053	−0.004
10c	−2.040	−2.053	0.013	−2.035	−0.005
10d[a]	0.016	0.031	−0.015	0.029	−0.013
10e[a]	−0.988	−1.547	0.559	−1.362	0.374
10f	−0.705	−0.684	−0.021	−0.696	−0.009
10g[a]	−1.026	−1.582	0.556	−1.564	0.538
11a	−2.012	−1.969	−0.043	−2.016	0.004
11b	−2.086	−2.102	0.016	−2.096	0.010
11c	−2.053	−2.083	0.030	−2.057	0.004
11d	−1.949	−1.986	0.037	−1.953	0.004
11e	−2.012	−2.023	0.011	−2.014	0.002
11f	−1.984	−1.957	−0.027	−1.986	0.002
12a	−2.152	−2.114	−0.038	−2.134	−0.018
12b	−2.016	−2.025	0.009	−2.013	−0.003
13a[a]	−0.732	−1.517	0.785	−0.986	0.254
13b	−2.003	−2.017	0.014	−2.004	0.001
13c[a]	−1.342	−1.298	−0.044	−1.132	−0.210

[a] Compounds taken for the test set.

activities than molecules without a substituent at this position (**9a, 12a** or **12b**). Two other small green contours were found around the phenyl ring at N_1-position of the imidazolidine-2,4-dione nucleus, implying that large substituents was positive around this position. This may be a reason why compounds **4a**–**4e, 5c**–**5f, 6e, 10a** and **10f** showed better potency than compounds without substituents at corresponding position (**6a**–**6c**). Some yellow regions located near the C_2, N_3 and C_4 positions of the imidazolidine-2,4-dione ring indicated that large substituents stretching into the domains bounded by four yellow contours might decrease the activity, which was in harmony with the fact that compounds **10c**, **11a**, **11b** (Fig. 5a), **11c**, **11d** and **11f** (Fig. 5b) displayed low activities. Interestingly, though compound **10d** was substituted by a bulky aromatic group (4-$CH_3OOCPhCH_2$) at R_1, the steric conformation of the large substituent avoided the yellow regions which were associated with unfavorable steric interactions, and hence compound **10d** still exhibited satisfactory activity (Fig. 6b). That also explained why compounds **4a**–**4e, 10a**, **10f**, **10g** and **13a** still showed good activities in spite of with a large R_1 substituent.

The CoMFA electrostatic interactions were displayed as blue and red contours, with the blue regions signifying areas of electropositive potential while red regions indicating areas of electronegative potential, and the results were illustrated in Fig. 3b. The electrostatic contour plots were discovered to be governed by red contours, suggesting a preference for electronegative substituents. The aromatic group of **5e** at N_1-position of the imidazolidine-2,4-dione ring was found to be embedded in a large red region and the other two red contours were observed near the benzene ring at C_5 position and the nitrogen atom at N_3-position of the imidazolidine-2,4-dione nucleus, respectively. This might be a powerful explanation to the high biological activity of **5e**. The other three small red areas close to para-position of the benzene ring linked to oxygen atom of common substructure of 39 imidazolidine-2,4-dione derivatives indicated that negatively charged substituents at this position was favored. This was supported by the fact that **10a** and **10d** with 4-CH_3OOC-$PhCH_2$ substituent at corresponding place possessed high potency. Also a blue contour favorable positively charged substitution was observed above aromatic nucleus in R_3 part, suggesting that electropositive substituents could be designed at this place to improve the PTP1B inhibitory potency of imidazolidine-2,4-dione derivatives.

The superiority of CoMSIA analysis is that Gaussian function is used to define the distance dependence. The influence of various properties contributing to the potency can be divided into spatial locations to identify the decisive areas to bioactivity and these can be visualized as contour maps. As a result, the CoMSIA contour maps, derived from using steric, electrostatic, hydrophobic, hydrogen bond donor, and hydrogen bond acceptor fields, were displayed in Fig. 4. CoMSIA steric and electrostatic contours were more or less similar to those of CoMFA, which were not displayed here.

Fig. 4a represented the CoMSIA hydrophobic field contribution and the yellow regions were associated with increased bioactivity. A major yellow polyhedron was discovered overlapping the plane of the 2,4-dichloro-substituted phenyl ring in part R_3 of compound **5e**, and another yellow region appeared around the phenyl ring in part R_2 of compound **5e**. The third large yellow polyhedron was under the imidazolidine-2,4-dione ring. Hydrophobic bulks were preferred at the above mentioned positions, which might explain why compound **5e** possessed the most potent activity and compounds with aromatic substituents at these positions showed better activities (**4a**–**4e, 5c**–**5f, 10c**–**10f** and **13a**). The correlations were consistent with the results of steric contours.

The CoMSIA hydrogen bond interactions were illustrated in Fig. 4b. Hydrogen bond donor field was depicted by cyan and purple contours. Cyan contours signified regions favoring hydrogen bond donors on ligands while purple contours indicated regions where hydrogen bond donor substituents on ligands were unfavorable for

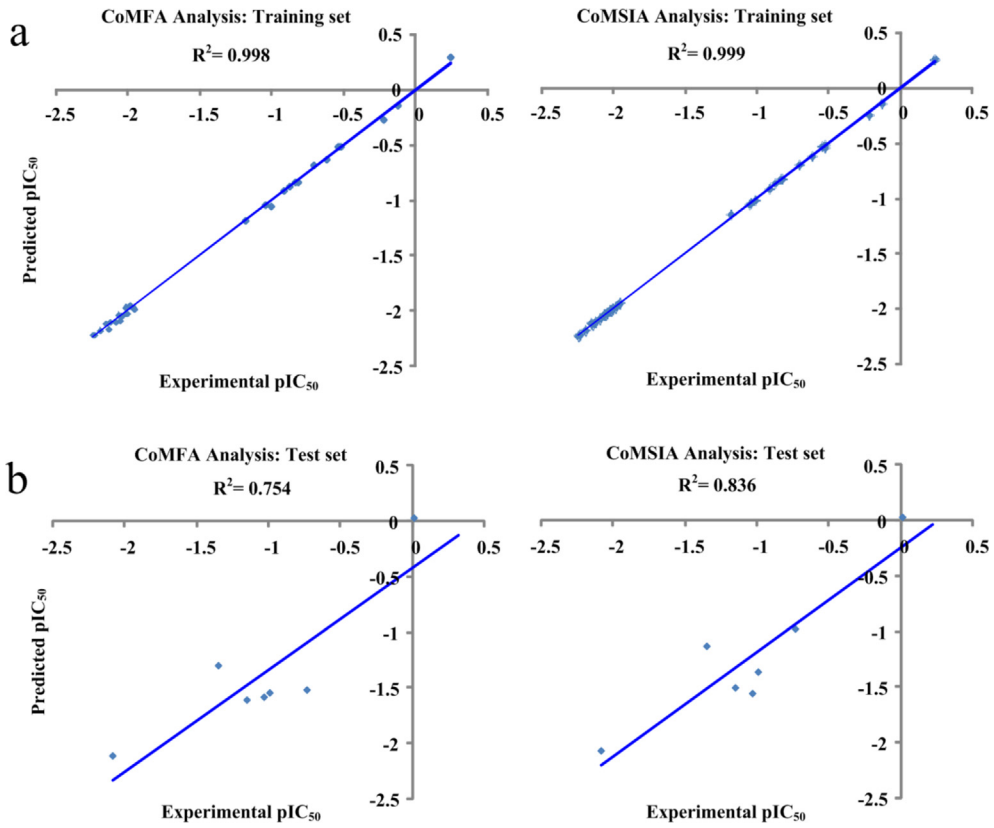

Fig. 2. CoMFA/CoMSIA predicted versus experimental pIC_{50} values. (a) Fitted predictions for the training set. (b) Fitted predictions for the test set.

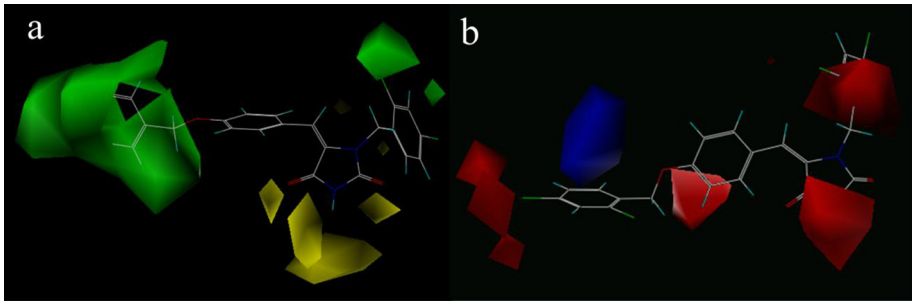

Fig. 3. CoMFA contour plots for steric field (a) and electrostatic field (b) with the most active compound **5e** as the reference molecule. (a) Sterically favored and disfavored regions are shown in green and yellow, respectively. (b) Electropositive favored and electronegative favored regions are shown in blue and red, respectively. (For interpretation of the references to color in this figure legend, the reader is referred to the web version of this article.)

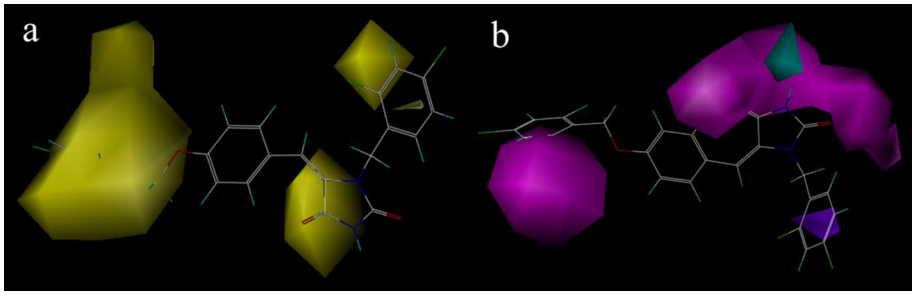

Fig. 4. CoMSIA contour plots for hydrophobic field (a) and H-bond interaction field (b) with the most active compound **5e** as the reference molecule. (a) Yellow polyhedra indicate regions where hydrophobic substituents are favored. (b) H-bond donors on ligand favored and disfavored are illustrated by cyan contours and purple contours, respectively, and H-bond acceptors on ligand favored are shown as magenta contours. (For interpretation of the references to color in this figure legend, the reader is referred to the web version of this article.)

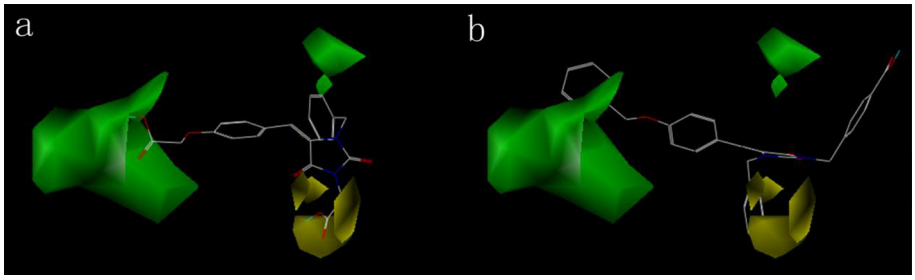

Fig. 5. CoMFA steric contours for less potent compounds: (a) compound **11b**, (b) compound **11f**.

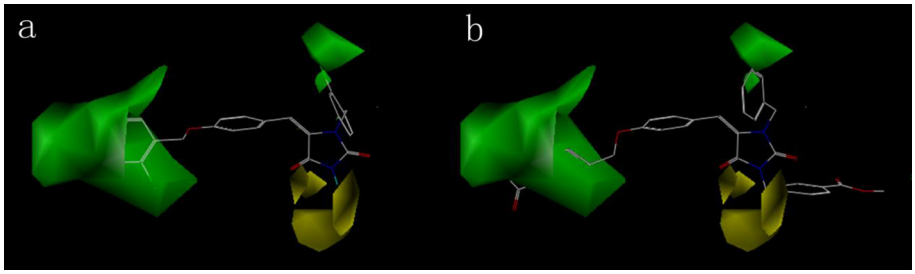

Fig. 6. CoMFA steric contours for highly potent compounds: (a) compound **5e**, (b) compound **10d**.

bioactivity. Besides, the magenta contours indicated hydrogen bond acceptor substituents on ligands were advantageous to activity. A cyan polyhedron was found near the nitrogen atom of the imidazolidine-2,4-dione ring, implying that hydrogen bond donor on inhibitors here was beneficial to activity. The presence of strong H-bond donor in compound **5e** was responsible for its high potency. Also, compounds with H-bond donors near these contours could observe a good range of activity (**5c**–**5f** and **6e**). However, a purple polyhedron appeared closely to the benzene ring of R_2 part of **5e**, indicating that hydrogen bond donors were not favored here. This was consistent with the interpretation of hydrophobic contours that hydrophilic substituents at this position decreased the pIC_{50} values. On the other side, a large magenta region surrounded two carbonyl oxygens at the C_2 and C_4 positions of the imidazolidine-2,4-dione ring, indicating that strong H-bond acceptors were crucial to the biological activity. This might powerfully support the importance of imidazolidine-2,4-dione scaffold to the high PTP1B affinity.

3.3. Docking analysis

Molecular docking could offer more insight into understanding the protein-inhibitor interactions [35–37]. Combined with docking results, we could further understand the important regions of imidazolidine-2,4-dione derivatives. The most active compound **5e** was found to bind in the same pocket and in the similar conformation of PTP1B receptor (PDB code: 2QBQ) that was occupied by the co-crystallized ligand 4B3, as shown in Fig. 7, which made our molecular docking in this paper more conceivable.

The structure of PTP1B consists of two binding sites: the catalytic active site (Cys215-Arg221) and the second phosphotyrosine binding site (Arg24, Arg254, Met258, Gly259, Gln262 and Gln266) [38]. Fig. 7a showed that large aromatic group at C_5 position of imidazolidine-2,4-dione ring of compounds **5e** and **10d** entered the deep and narrow catalytic pocket. This was consistent with the 3D-QSAR contour that a bulky hydrophobic group was beneficial to bioactivity at this place. On one hand, the aromatic ring at N_1-position of imidazolidine-2,4-dione nucleus of compound **5e** entered the second phosphotyrosine binding site. On the other hand, the aryl group at R_1 of compound **10d** also perfectly matched with the second binding site. This may be a reason why compounds **5e** and **10d** showed high potency. As a common substructure, imidazolidine-2,4-dione ring of compound **5e** formed intense interactions with binding site, including hydrogen bonds with Arg254, Arg24 and Gly259, respectively, and non-bonded interactions (Fig. 7b). However, compound **10d** only formed weaker interactions (van der Waals interactions, hydrophobic interactions, etc.). That might lead to lower bioactivity of compound **10d** than compound **5e**.

4. Conclusion

In summary, a series of imidazolidine-2,4-dione derivatives was synthesized and evaluated for the PTP1B inhibitory activities. A 3D-QSAR study using CoMFA and CoMSIA methods was applied to study the structure-activity relationship and the results were as follows: (1) large groups at the C_5 position of imidazolidine-2,4-dione ring was beneficial to bioactivity; (2) a hydrophobic, electronegative and bulky substitutes at N_1 position of imidazolidine-2,4-dione nucleus was necessary to activity; (3) two carbonyl oxygens at the C_2 and C_4 positions of the imidazolidine-2,4-dione ring was crucial to the biological activity. The above results were completely consistent with the subsequent docking analysis. The combined 3D-QSAR and docking studies could provide useful information about the action mechanism between ligand and target, and guide further modification of imidazolidine-2,4-dione derivatives.

5. Experimental section

5.1. Chemistry

All the reagents were purchased from commercial suppliers and were used without further purification unless otherwise indicated. Reaction courses were monitored by TLC on silica gel pre-coated F_{254} Merck plates. ^1H NMR spectra was taken on a Bruker spectrometer using TMS as the internal standard, and DMSO-d_6 was

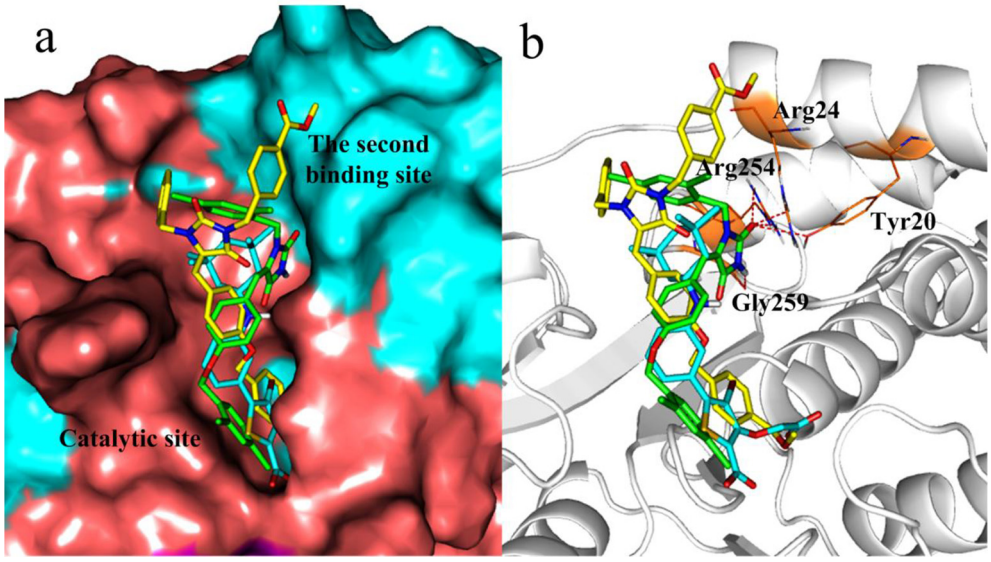

Fig. 7. Docking of compound **5e** (green), **10d** (yellow) and co-crystallized ligand 4B3 (cyan) with PTP1B. (a) Surface representation of PTP1B in complex with **5e**, **10d** and 4B3. (b) Docking interactions of compound **5e**, **10d** and 4B3 with PTP1B active site. The H-bond interactions between PTP1B and **5e** were shown as red dashed lines. (For interpretation of the references to color in this figure legend, the reader is referred to the web version of this article.)

used as the solvent. Mass spectra were measured on an Agilent 1100 series.

*5.1.1. General procedure for the synthesis of **4a–4e**, **5a–5f** and **6a–6h***

4-hydroxybenzaldehyde (50 mmol) and hydantoin (55 mmol) were dissolved in 10 ml piperidine. The mixture was heated to 130 °C for 0.5 h, and TLC analysis indicated that the reaction was complete. Water (200 ml) was added to the mixture after it was cooled to the room temperature. Then, stirring until the mixture was dissolved and filtrating to remove the undissolved substance. Subsequently, 20 ml10 N HCl was dropwise added to the filtrate and the precipitate was filtrated, washed with water and dried to give compound **3**.

A mixture of 5-(4-hydroxybenzylidene)imidazolidine-2,4-dione (**3**) (20 mmol), ethyl 2-bromoacetate (20 mmol), K_2CO_3 (20 mmol) and acetone (120 ml) was refluxed for 24 h. After the reaction was complete detected by TLC analysis, the mixture was filtrated to remove the inorganic salt and concentrated under vacuo. The resulting residue was purified by column chromatography to give **5b** and **6b**.

5-(4-hydroxybenzylidene)imidazolidine-2,4-dione (**3**) (2 mmol), organochlorine compound (1.83 mmol) and NaH (6.47 mmol) were added in 8.6 ml DMF. The mixture was heated to 70 °C for 4 h, and TLC analysis showed that the reaction was complete. The mixture was extracted by ethyl acetate, and the combined organic layer was washed with saturated brine, dried over anhydrous $MgSO_4$, filtered, and concentrated. The resulting residue was purified by silica gel column chromatography to give the target compounds **4a–4e, 5a, 5c–5f, 6a** and **6c–6h**.

*5.1.1.1. 5-(4-hydroxybenzylidene)imidazolidine-2,4-dione(**3**).* A yellow solid with the following characteristics: 79.5% yield; m.p. 316–318 °C; ^{1}H NMR (DMSO-d_6, 400 Hz): δ 11.089 (s, 1H, N_1H); 10.299 (s, 1H, N_3H); 9.856 (s, 1H, OH); 7.469 (d, 2H, J = 8.4 Hz, Ar–H); 6.767 (q, 2H, J = 8.4 Hz, Ar–H); 6.346 (s, 1H, Ar-CH); MS (*m/z*): 205.0 (M + 1).

*5.1.1.2. Ethyl 2-(5-(4-(2-ethoxy-2-oxoethoxy)benzylidene)-2,4-dioxoimidazolidin-1-yl) acetate(**5b**).* A yellow solid with the following characteristics: 20.91% yield; m.p. 158–160 °C; ^{1}H NMR (DMSO-*d6*, 400 Hz): δ 10.858 (s, 1H, N_3H); 7.635 (d, 2H, J = 9.2 Hz, Ar–H); 6.984 (d, 2H, J = 8.8 Hz, Ar–H); 6.876 (s, 1H, =CH); 4.849 (s, 2H, Ar–O–CH_2); 4.304 (s, 2H, N_1–CH_2); 4.162 (q, 4H, J = 7.2 Hz, OCH_2); 1.217 (m, 6H, CH_3); MS (*m/z*): 377.2 (M + 1).

*5.1.1.3. Ethyl 2-(4-((2,5-dioxoimidazolidin-4-ylidene)methyl)phenoxy)acetate(**6b**).* A white solid with the following characteristics: 11.27% yield; m.p. 229–230 °C; ^{1}H NMR (DMSO-d_6, 400 Hz): δ 10.727 (s, 1H, N_1H); 9.923 (s, 1H, N_3H); 7.526 (d, 2H, J = 8.8 Hz, Ar–H); 6.811 (d, 2H, J = 8.4 Hz, Ar–H); 6.544 (s, 1H, =CH); 4.293 (s, 2H, Ar–O–CH_2); 4.158 (q, 4H, J = 7.2 Hz, OCH_2); 1.210 (m, 3H, CH_3); MS (*m/z*): 291.2 (M + 1).

*5.1.1.4. 1,3-bis(2-chlorobenzyl)-5-(4-((2-chlorobenzyl)oxy)benzylidene)imidazolidine-2,4-dione(**4a**).* A white solid with the following characteristics: 24.94% yield; m.p. 134–136 °C; ^{1}H NMR (DMSO-d_6, 400 Hz): δ 7.475–7.515 (m, 3H, Ar–H); 7.331–7.391 (m, 4H, Ar–H); 7.205 (q, 3H, J = 7.2 Hz, Ar–H); 7.011 (t, 3H, J = 8.4 Hz, Ar–H); 6.860 (t, 3H, J = 8.8 Hz, Ar–H); 5.735 (s, 1H, =CH); 5.123 (s, 2H, OCH_2); 4.840 (s, 2H, N_1–CH_2); 4.718 (s, 2H, N_3–CH_2); MS (*m/z*): 577.0 (M + 1).

*5.1.1.5. 5-(4-(2-oxo-2-phenylethoxy)benzylidene)-1,3-bis(2-oxo-2-phenylethyl)imidazolidine-2,4-dione(**4b**).* A white solid with the following characteristics: 6.71% yield; m.p. 153–155 °C; ^{1}H NMR (DMSO-d_6, 400 Hz): δ 8.093 (t, 2H, J = 7.2 Hz, Ar–H); 7.947 (t, 2H, J = 7.2 Hz, Ar–H); 7.556–7.755 (m, 9H, Ar–H); 7.493 (t, 2H, J = 7.6 Hz, Ar–H); 7.203 (d, 2H, J = 8.8 Hz, Ar–H); 6.854 (s, 1H, = CH); 6.784 (d, 2H, J = 8.8 Hz, Ar–H); 5.404 (s, 2H, $COCH_2$); 5.243 (s, 2H, $COCH_2$); 5.112 (d, 4H, OCH_2); MS (*m/z*): 559.0 (M + 1).

*5.1.1.6. 1,3-bis(4-methoxybenzyl)-5-(4-((4-methoxybenzyl)oxy)benzylidene)imidazolidine-2,4-dione(**4c**).* A white solid with the following characteristics: 34% yield; m.p. 129–131 °C; ^{1}H NMR (DMSO-d_6, 400 Hz): δ 7.384 (d, 2H, J = 8.8 Hz, Ar–H); 7.212 (t, 4H, J = 8.8 Hz, Ar–H); 6.943 (m, 6H, Ar–H); 6.722 (s, 1H, =CH); 6.619

(d, 2H, J = 8.4 Hz, Ar–H); 6.451 (d, 2H, J = 8.4 Hz, Ar–H); 5.074 (s, 2H, OCH_2); 4.654 (d, 4H, J = 6.8 Hz, NCH_2); 3.732 (s, 6H, OCH_3); 3.643 (s, 3H, OCH_3); MS (m/z): 565.2 (M + 1).

*5.1.1.7. 1,3-bis(2,4-dichlorobenzyl)-5-(4-((2,4-dichlorobenzyl)oxy) benzylidene)imidazolidine-2,4-dione(**4d**).* A white solid with the following characteristics: 18.86% yield; m.p. 168–169 °C; ^{1}H NMR (DMSO-d_6,400 Hz): δ 6.769–7.673 (m, 14H, Ar–H, =CH); 5.094 (s, 2H, Ar–O–CH_2); 4.769 (s, 2H, N_1–CH_2); 4.630 (s, 2H, N_3–CH_2); MS (m/z): 682.9 (M + 1).

*5.1.1.8. 1,3-bis(3,4-dichlorobenzyl)-5-(4-((3,4-dichlorobenzyl)oxy) benzylidene)imidazolidine-2,4-dione(**4e**).* A pale yellow solid with the following characteristics: 23.7% yield; m.p. 139–140 °C; ^{1}H NMR (DMSO-d_6, 400 Hz): δ 7.596–7.719 (m, 4H, Ar–H); 7.452 (q, 1H, J = 6.4 Hz, Ar–H); 7.320 (d, 2H, J = 8.0 Hz, Ar–H); 7.104 (d, 2H, J = 8.4 Hz, Ar–H); 6.922 (d, 2H, J = 8.8 Hz, Ar–H); 6.753 (s, 2H, Ar–H); 5.738 (s, 1H, =CH); 5.149 (s, 2H, NCH_2); 4.743 (s, 2H, NCH_2); 4.699 (s, 2H, OCH_2); MS (m/z): 696.0 (M + NH_4).

*5.1.1.9. 1-benzyl-5-(4-(benzyloxy)benzylidene)imidazolidine-2,4-dione(**5a**).* A white solid with the following characteristics: 26% yield; m.p. 231–233 °C; ^{1}H NMR (DMSO-d_6, 400 Hz): δ 10.740 (s, 1H, N_3H); 7.614 (d, 2H, J = 8.8 Hz, Ar–H); 7.449 (d, 2H, J = 7.2 Hz, Ar–H); 7.379 (q, 2H, J = 7.6 Hz, Ar–H); 7.270–7.342 (m, 6H, Ar–H); 7.043 (d, 2H, J = 8.8 Hz, Ar–H); 6.540 (s, 1H, =CH); 5.145 (d, 2H, J = 8.4 Hz, OCH_2); 4.654 (s, 2H, CH_2); MS (*m/z*): 383.0 (M–1).

*5.1.1.10. 1-(4-chlorobenzyl)-5-(4-((4-chlorobenzyl)oxy)benzylidene) imidazolidine-2,4-dione(**5c**).* A pale yellow solid with the following characteristics: 27% yield; m.p. 167–168 °C; ^{1}H NMR (DMSO-d_6, 400 Hz): δ 9.867 (s, 1H, N_3H); 7.310–7.434 (m, 9H, Ar–H); 6.680–6.734 (m, 2H, Ar–H); 6.429 (s, 1H, =CH); 4.938 (s, 2H, $ArCH_2$); 4.720 (t, 2H, J = 6.4 Hz, OCH_2); MS (*m/z*): 452.0 (M–1).

*5.1.1.11. 1-(3,4-dichlorobenzyl)-5-(4-((3,4-dichlorobenzyl)oxy)benzylidene)imidazolidine-2,4-dione(**5d**).* A white solid with the following characteristics: 49% yield; m.p. 242–244 °C; ^{1}H NMR (DMSO-d_6, 400 Hz): δ 9.876 (s, 1H, N_3H); 7.841 (d, 2H, J = 8.4 Hz, Ar–H); 7.595–7.660 (m, 4H, Ar–H); 7.305–7.358 (m, 2H, Ar–H); 6.730 (d, 2H, J = 8.8 Hz, Ar–H); 6.426 (s, 1H, =CH); 4.945 (s, 2H, Ar–O–CH_2); 4.725 (s, 2H, N_1–CH_2); MS (*m/z*): 521.0 (M–1).

*5.1.1.12. 1-(2,4-dichlorobenzyl)-5-(4-((2,4-dichlorobenzyl)oxy)benzylidene)imidazolidine-2,4-dione(**5e**).* A pale yellow solid with the following characteristics: 38% yield; m.p. 261–262 °C; ^{1}H NMR (DMSO-d_6, 400 Hz): δ 9.888 (s, 1H, N_3H); 7.840 (d, 2H, J = 8.8 Hz, Ar–H); 7.669 (q, 2H, J = 12.0 Hz, Ar–H); 7.308–7.429 (m, 4H, Ar–H); 6.724 (d, 2H, J = 8.8 Hz, Ar–H); 6.361 (s, 1H, =CH); 4.969 (s, 2H, Ar–O–CH_2); 4.777 (s, 2H, N_1–CH_2); MS (*m/z*): 519.0 (M–1).

*5.1.1.13. 5-(4-(benzyloxy)benzylidene)imidazolidine-2,4-dione(**6a**).* A pale gray solid with the following characteristics: 9% yield; m.p. 285–288 °C; ^{1}H NMR (DMSO-d_6, 400 Hz): δ 10.638 (s, 1H, N_3H); 9.886 (s, 1H, N_1H); 7.500 (d, 2H, J = 8.8 Hz, Ar–H); 7.267–7.353 (q, 4H, Ar–H); 6.789 (d, 2H, J = 8.8 Hz, Ar–H); 6.505 (s, 1H, =CH); 4.651 (s, 2H, CH_2); MS (*m/z*): 293.0 (M–1).

*5.1.1.14. 5-(4-(2-oxo-2-phenylethoxy)benzylidene)imidazolidine-2,4-dione(**6c**).* A yellow solid with the following characteristics: 12% yield; m.p. 251–252 °C; ^{1}H NMR (DMSO-d_6, 400 Hz): δ 10.730 (s, 1H, N_3H); 9.919 (s, 1H, N_1H); 8.068 (d, 2H, J = 7.2 Hz, Ar–H); 7.724 (t, 1H, J = 7.6 Hz, Ar–H); 7.528–7.606 (m, 4H, Ar–H); 6.813 (d, 2H, J = 8.8 Hz, Ar–H); 6.548 (s, 1H, =CH); 5.096 (s, 2H, OCH_2); MS(m/z): 323.2 (M + 1).

*5.1.1.15. 5-(4-((2-chlorobenzyl)oxy)benzylidene)imidazolidine-2,4-dione(**6d**).* A white solid with the following characteristics: 12% yield; m.p. 265–268 °C; ^{1}H NMR (DMSO-d_6, 400 Hz): δ 11.135 (s, 1H, N_3H); 10.428 (s, 1H, N_1H); 7.376–7.604 (m, 6H, Ar–H); 7.046 (d, 2H, Ar–H); 6.381 (s, 1H, =CH); 5.201 (s, 2H, OCH_2); MS (*m/z*): 329.0 (M + 1).

*5.1.1.16. 5-(4-((2,4-dichlorobenzyl)oxy)benzylidene)imidazolidine-2,4-dione(**6e**).* A yellow solid with the following characteristics: 12% yield; m.p. 241–242 °C; ^{1}H NMR (DMSO-d_6, 400 Hz): δ 10.719 (s, 1H, N_3H); 9.905 (s, 1H, N_1H); 7.648 (d, 1H, J = 2.0 Hz, Ar–H); 7.518 (t, 2H, Ar–H); 7.400 (q, 1H, J = 6.0 Hz, Ar–H); 7.248 (d, 1H, J = 6.0 Hz, Ar–H); 6.797 (d, 2H, J = 8.4 Hz, Ar–H); 6.523 (s, 1H, =CH); 4.706 (s, 2H, OCH_2); MS (*m/z*): 362.0 (M–1).

*5.1.1.17. 5-(4-((4-chlorobenzyl)oxy)benzylidene)imidazolidine-2,4-dione(**6f**).* A white solid with the following characteristics: 14% yield; m.p. 255–258 °C; ^{1}H NMR (DMSO-d_6, 400 Hz): δ 10.654 (s, 1H, N_3H); 9.895 (s, 1H, N_1H); 7.499 (s, 2H, J = 8.8 Hz, Ar–H); 7.381–7.415 (m, 2H, Ar–H); 7.303 (d, 2H, J = 8.4 Hz, Ar–H); 6.786 (d, 2H, J = 8.8 Hz, Ar–H); 6.502 (s, 1H, =CH); 4.641 (s, 2H, OCH_2); MS (*m/z*): 329.0 (M + 1).

*5.1.1.18. 5-(4-(3-phenylpropoxy)benzylidene)imidazolidine-2,4-dione(**6g**).* A pale yellow solid with the following characteristics: 12% yield; m.p. 246–249 °C; ^{1}H NMR (DMSO-d_6, 400 Hz): δ 10.519 (s, 1H, N_3H); 9.864 (s, 1H, N_1H); 7.485 (d, 2H, J = 8.4 Hz, Ar–H); 7.143–7.284 (m, 5H, Ar–H); 6.773 (t, 2H, J = 7.2 Hz, Ar–H); 6.453 (s, 1H, =CH); 3.486 (t, 2H, J = 7.2 Hz, OCH_2); 2.586 (t, 2H, J = 7.2 Hz, $PhCH_2$); 1.823–1.896 (m, 2H, $PhCH_2CH_2$); MS (*m/z*): 323 (M + 1).

*5.1.1.19. 5-(4-((3,4-dichlorobenzyl)oxy)benzylidene)imidazolidine-2,4-dione(**6h**).* A yellow solid with the following characteristics: 9% yield; m.p. 236–238 °C; ^{1}H NMR (DMSO-d_6, 400 Hz): δ 10.671 (s, 1H, N_3H); 9.909 (s, 1H, N_1H); 7.576 (q, 2H, J = 7.6 Hz, Ar–H); 7.511 (d, 2H, J = 8.4 Hz, Ar–H); 7.269 (q, 1H, J = 6.0 Hz, Ar–H); 6.790 (d, 1H, J = 8.4 Hz, Ar–H); 6.511 (s, 1H, =CH); 4.658 (s, 2H, OCH_2); MS (*m/z*): 360.9 (M–1).

*5.1.2. General procedure for the synthesis of **9a** and **9b***

A mixture of benzyl hydantoin (4 mmol), methyl bromoacetate (or methyl 4-(bromomethyl) benzoate) (4 mmol) and K_2CO_3 (4 mmol) in 30 ml DMF was heated to 85 °C for 3 h. After completion of the reaction as monitored by TLC, The mixture was filtrated to remove the solid. The filtrate was concentrated under vacuo, extracted by ethyl acetate and dried over anhydrous $MgSO_4$. The resulting residue was purified using silica gel column chromatography with petroleum ether: ethyl acetate = 8:1–4:1 to give methyl 2-(3-benzyl-2,5-dioxoimidazolidin-1-yl)acetate (**8a**) (or methyl 4-((3-benzyl-2,5-dioxoimidazolidin-1-yl)methyl)benzoate (**8b**)). Subsequently, the mixture of compound **8a** (or **8b**) (3.2 mmol) and 4-hydroxybenzaldehyde (3.2 mmol) in 25 ml of toluene was treated with 2 ml piperidine and 2 ml acetic acid. The reaction mixture was heated at reflux for 4.5 h and then concentrated via rotary evaporator to afford the crude product. The resulting residue was purified by silica gel column chromatography to give **9a** (or **9b**).

*5.1.2.1. Methyl 2-(3-benzyl-2,5-dioxoimidazolidin-1-yl)acetate(**8a**).* A colorless oil with the following characteristics: 77.41% yield; ^{1}H NMR (DMSO-d_6, 400 MHz): δ 7.379–7.268 (5H, m, Ar–H); 4.534 (2H, s, N–CH_2); 4.246 (2H, s, N–CH_2); 4.018 (2H, s, N–CH_2); 3.691 (3H, s, OCH_3); MS (*m/z*): 280.1 (M + NH_4).

*5.1.2.2. Methyl 4-((3-benzyl-2,5-dioxoimidazolidin-1-yl)methyl)benzoate(**8b**).* A colorless oil with the following characteristics: 80.25% yield; ^{1}H NMR (DMSO-d_6, 400 MHz): δ 7.941 (2H, t, J = 8.40 Hz, Ar–H); 7.721 (2H, t, J = 8.00 Hz, Ar–H); 7.388–7.684 (5H, m, Ar–H); 4.467 (2H, s, N–CH_2); 4.529 (2H, s, N–CH_2); 3.992 (2H, s, N–CH_2); 3.885 (3H, s, OCH_3); MS (*m/z*): 356.1 (M + NH_4).

*5.1.2.3. (E)-Methyl 2-(3-benzyl-4-(4-hydroxybenzylidene)-2,5-dioxoimidazolidin-1-yl)acetate(**9a**).* A yellow solid with the following characteristics: 27.04% yield; m.p. 205.3–205.8 °C; ^{1}H NMR (DMSO-d_6, 400 MHz): δ 9.956 (1H, s, Ar–OH); 7.834 (2H, d, J = 8.64 Hz, Ar–H); 7.392–7.281 (5H, m, Ar–H); 6.746 (2H, d, J = 8.64 Hz, Ar–H); 6.515 (1H, s, =CH); 4.988 (2H, s, N–CH_2); 4.411 (2H, s, N–CH_2); 3.716 (3H, s, OCH_3); MS (*m/z*): 367.1 (M + 1).

*5.1.2.4. (E)-Methyl 4-((3-benzyl-4-(4-hydroxybenzylidene)-2,5-dioxoimidazolidin-1-yl)methyl)benzoate(**9b**).* A yellow solid with the following characteristics: 25.28% yield; m.p. 197.5–197.9 °C; ^{1}H NMR (DMSO-d_6, 400 MHz): δ 9.913 (1H, s, Ar–OH); 7.955 (2H, d, J = 8.00 Hz, Ar–H); 7.836 (2H, d, J = 8.80 Hz, Ar–H); 7.356–7.477 (5H, m, Ar–H); 7.293 (2H, d, J = 8.00 Hz, Ar–H); 6.731 (2H, d, J = 8.40 Hz, Ar–H); 6.469 (1H, s, =CH); 4.970 (2H, s, N–CH_2); 4.817 (2H, s, N–CH_2); 3.847 (3H, s, OCH_3); MS (m/z): 460.2 (M + NH_4).

5.1.3. General procedure for the synthesis of 10a-10f

A mixture of **9a** (or **9b**) (2 mmol), methyl 4-(bromomethyl) benzoate (or methyl bromoacetate or benzyl chloride) (2 mmol) and K_2CO_3 (2 mmol) in 50 ml DMF was stirred at 85 °C for 3 h, and TLC analysis indicated the reaction was complete. Then, the mixture was filtrated and the filtrate was concentrated under vacuo, extracted by ethyl acetate and dried over anhydrous $MgSO_4$. The resulting residue was purified by silica gel column chromatography with petroleum ether: ethyl acetate = 8:1–4:1 to give **10a**–**10c** (or **10d**–**10f**).

*5.1.3.1. (E)-Methyl 4-((4-((3-benzyl-1-(2-methoxy-2-oxoethyl)-2,5-dioxoimidazolidin-4-ylidene)methyl)phenoxy)methyl)benzoate(**10a**).* A white solid with the following characteristics: 70.42% yield; m.p. 145.5–146.2 °C; ^{1}H NMR (DMSO-d_6, 400 MHz): δ 7.930 (4H, t, J = 9.44 Hz, Ar–H); 7.583 (4H, d, J = 7.84 Hz, Ar–H); 7.372–7.011 (5H, m, Ar–H); 6.571 (1H, s, =CH); 5.241 (2H, s, N–CH_2); 4.993 (2H, s, CH_2); 4.408 (2H, s, N–CH_2); 3.852 (3H, s, OCH_3); 3.714 (3H, s, OCH_3); MS (*m/z*): 532.2 (M + NH_4).

*5.1.3.2. (E)-Methyl 2-(4-((3-benzyl-1-(2-methoxy-2-oxoethyl)-2,5-dioxoimidazolidin-4-ylidene)methyl)phenoxy)acetate(**10b**).* A white solid with the following characteristics: 69.33% yield; m.p. 136.9–137.4 °C; ^{1}H NMR (DMSO-d_6, 400 MHz): δ 7.888 (2H, d, J = 8.44 Hz, Ar–H); 7.393–7.283 (5H, m, Ar–H); 6.928 (2H, d, J = 8.44 Hz, Ar–H); 6.5739 (1H, s, =CH); 4.994 (2H, s, N–CH_2); 4.836 (2H, s, CH_2); 4.408 (2H, s, N–CH_2); 3.7141 (3H, s, OCH_3); 3.6901 (3H, s, OCH_3); MS (*m/z*): 360.9 (M–1).

*5.1.3.3. (E)-Methyl 2-(3-benzyl-4-(4-(benzyloxy)benzylidene)-2,5-dioxoimidazolidin-1-yl)acetate(**10c**).* A yellow solid with the following characteristics: 79.86% yield; m.p. 112.7–113.9 °C; ^{1}H NMR (DMSO-d_6, 400 MHz): δ 7.404 (2H, d, J = 0.80 Hz, Ar–H); 7.359–7.385 (5H, m, Ar–H); 7.325–7.360 (5H, m, Ar–H); 7.010 (2H, d, J = 8.80 Hz, Ar–H); 6.565 (1H, s, =CH); 5.131 (2H, s, N–CH_2); 4.994 (2H, s, O–CH_2); 4.413 (2H, s, N–CH_2); 3.371 (3H, s, OCH_3); MS (*m/z*): 474.2 (M + NH_4).

*5.1.3.4. (E)-Methyl 4-((4-((3-benzyl-1-(4-(methoxycarbonyl)benzyl)-2,5-dioxoimidazolidin-4-ylidene)methyl)phenoxy)methyl)benzoate(**10d**).* A pale yellow solid with the following characteristics: 75.83% yield; m.p. 175.6–176.4 °C; ^{1}H NMR (DMSO-d_6, 400 MHz): δ 8.000 (2H, d, J = 8.00 Hz, Ar–H); 7.882 (2H, d, J = 8.80 Hz, Ar–H); 7.511 (2H, d, J = 8.00 Hz, Ar–H); 7.470 (2H, d, J = 8.00 Hz, Ar–H); 7.364 (2H, d, J = 7.20 Hz, Ar–H); 7.333–7.460 (5H, m, Ar–H); 6.911 (2H, d, J = 8.00 Hz, Ar–H); 6.189 (1H, s, =CH); 5.126 (2H, s, N–CH_2); δ 4.927 (2H, s, N–CH_2); 4.861 (2H, s, O–CH_2); 3.926 (3H, s, OCH_3); 3.906 (3H, s, OCH_3); MS (*m/z*): 608.3 (M + NH_4).

*5.1.3.5. (E)-Methyl 4-((3-benzyl-4-(4-(2-methoxy-2-oxoethoxy)benzylidene)-2,5-dioxoimidazolidin-1-yl)methyl)benzoate(**10e**).* A white solid with the following characteristics: 66.87% yield; m.p. 161.7–162.6 °C; ^{1}H NMR (DMSO-d_6, 400 MHz): δ 7.610(2H, d, J = 8.00 Hz, Ar–H); 7.352 (2H, d, J = 1.60 Hz, Ar–H); 7.326 (2H, d, J = 7.20 Hz, Ar–H); 7.255–7.290 (5H, m, Ar–H); 6.855 (2H, d, J = 8.80 Hz, Ar–H); 6.182 (1H, s, =CH); 4.927 (2H, s, N–CH_2); 4.861 (2H, s, N–CH_2); 4.633 (2H, s, CH_2); 3.905 (3H, s, OCH_3); 3.712 (3H, s, OCH_3); MS (*m/z*): 532.2 (M + NH_4).

*5.1.3.6. (E)-Methyl 4-((3-benzyl-4-(4-(benzyloxy)benzylidene)-2,5-dioxoimidazolidin-1-yl)methyl)benzoate(**10f**).* A white solid with the following characteristics: 82.74% yield; m.p. 154.4–154.9 °C; ^{1}H NMR (DMSO-d_6, 400 MHz): δ 7.427 (2H, d, J = 10.0 Hz, Ar–H); 7.400 (2H, d, J = 8.40 Hz, Ar–H); 7.343–7.381 (5H, m, Ar–H); 7.277–7.340 (5H, m, Ar–H); 7.340 (2H, d, J = 4.28 Hz, Ar–H); 6.517 (1H, s, =CH); 5.127 (2H, s, N–CH_2); 4.972 (2H, s, N–CH_2); 4.813 (2H, s, CH_2); 3.846 (3H, s, OCH_3); MS (*m/z*): 550.2 (M + NH_4).

*5.1.4. General procedure for the synthesis of **11a**-**11f***

A mixture of **10a-10f** (1 mmol), 15 ml NaOH (1 mol/L) and 15 ml methanol was refluxed for 3.5 h. After completion of the reaction as monitored by TLC, the pH of the mixture was regulated to 3–5 by hydrochloric acid (1 mol/L). Then, the mixture was extracted by ethyl acetate, dried over anhydrous $MgSO_4$ and evaporated to give **11a-11f**.

*5.1.4.1. (E)-4-((4-((3-benzyl-1-(carboxymethyl)-2,5-dioxoimidazolidin-4-ylidene)methyl)phenoxy)methyl)benzoic acid(**11a**).* A white solid with the following characteristics: 23.05% yield; m.p. 155.6–156.3 °C; ^{1}H NMR (DMSO-d_6, 400 MHz): δ 12.632 (2H, s, COOH); 7.975 (2H, d, J = 7.96 Hz, Ar–H); 7.570–7.506 (5H, m, Ar–H); 7.090 (4H, t, J = 7.46 Hz, Ar–H); 6.910 (2H, d, J = 8.52 Hz, Ar–H); 6.625 (1H, s, =CH); 5.229 (2H, s, N–CH_2); 4.594 (2H, s, CH_2); 4.323 (2H, s, N–CH_2); MS (*m/z*): 505.0 (M + NH_4).

*5.1.4.2. (E)-2-(4-((3-benzyl-1-(carboxymethyl)-2,5-dioxoimidazolidin-4-ylidene)methyl)phenoxy)acetic acid(**11b**).* A white solid with the following characteristics: 20.43% yield; m.p. 132.6–133.2 °C; ^{1}H NMR (DMSO-d_6, 400 MHz): δ 12.632 (2H, s, COOH); 7.509 (2H, d, J = 8.44 Hz. Ar–H); 7.098 (5H, m, Ar–H); 6.800 (2H, d, J = 8.60 Hz, Ar–H); 6.628 (1H, s, =CH); 4.695 (2H, s, N–CH_2); 4.570 (2H, s, N–CH_2); 4.350–4.001 (2H, m, O–CH_2); MS (*m/z*): 409.1 (M–1).

*5.1.4.3. (E)-2-(3-benzyl-4-(4-(benzyloxy)benzylidene)-2,5-dioxoimidazolidin-1-yl)acetic acid(**11c**).* A white solid with the following characteristics: 61.32% yield; m.p. 173.9–174.3 °C; ^{1}H NMR (DMSO-d_6, 400 MHz): δ 13.249 (1H, s, COOH), 7.910 (2H, d, J = 8.84 Hz, Ar–H); 7.367–7.451 (5H, m, Ar–H); 7.280–7.343 (5H, m, Ar–H); 7.108 (2H, d, J = 8.80 Hz, Ar–H); 6.546 (1H, s, =CH); 5.132 (2H, s, N–CH_2); 4.987 (2H, s, O–CH_2); 4.272 (2H, s, N–CH_2); MS (*m/z*): 460.2 (M + NH_4).

*5.1.4.4. (E)-4-((4-((3-benzyl-1-(4-carboxybenzyl)-2,5-dioxoimidazolidin-4-ylidene)methyl)phenoxy)methyl)benzoic acid(**11d**).* A white solid with the following characteristics: 27.45%

yield; m.p. 184.3–185.0 °C; ^{1}H NMR (DMSO-d_6, 400 MHz): δ 12.819 (2H, s, COOH); 7.977 (2H, d, J = 8.40 Hz, Ar–H); 7.957 (2H, d, J = 6.00 Hz, Ar–H); 7.885 (2H, d, J = 8.80 Hz, Ar–H); 7.762 (2H, d, J = 8.00 Hz, Ar–H); 7.580 (2H, d, J = 8.00 Hz, Ar–H); 7.188–7.432 (5H, m, Ar–H); 7.187 (2H, d, J = 8.00 Hz, Ar–H); 6.189 (1H, s, =CH); 5.335 (2H, s, N–CH_2); 5.216 (2H, s, N–CH_2); 5.181 (2H, s, O–CH_2).

*5.1.4.5. (E)-4-((3-benzyl-4-(4-(carboxymethoxy)benzylidene)-2,5-dioxoimidazolidin-1-yl)methyl)benzoic acid(**11e**).* A white solid with the following characteristics: 35.47% yield; m.p. 144.6–145.3 °C; ^{1}H NMR (DMSO-d_6, 400 MHz): δ 12.985 (2H, s, COOH); 7.926 (2H, d, J = 8.40 Hz, Ar–H); 7.894 (2H, d, J = 8.80 Hz, Ar–H); 7.410 (2H, d, J = 8.40 Hz, Ar–H); 7.362–7.372 (5H, m, Ar–H); 6.892 (2H, d, J = 8.80 Hz, Ar–H); 6.524 (1H, s, =CH); 4.974 (2H, s, N–CH_2); 4.805 (2H, s, N–CH_2); 4.699 (2H, s, CH_2); MS (m/z): 504.1 (M + NH_4).

*5.1.4.6. (E)-4-((3-benzyl-4-(4-(benzyloxy)benzylidene)-2,5-dioxoimidazolidin-1-yl)methyl)benzoic acid(**11f**).* A white solid with the following characteristics: 65.65% yield; m.p. 173.7–173.9 °C; ^{1}H NMR (DMSO-d_6, 400 MHz): δ 12.742 (1H, s, COOH), 7.762 (2H, d, J = 8.00 Hz, Ar–H); 7.486 (2H, d, J = 9.60 Hz, Ar–H); 7.423–7.473 (5H, m, Ar–H); 7.342–7.409 (5H, m, Ar–H); 7.197 (2H, d, J = 4.4 0 Hz, Ar–H); 6.899 (1H, s, =CH); 5.122 (2H, s, N–CH_2); 4.729 (2H, s, N–CH_2); 4.339 (2H, s, CH_2); MS (m/z): 537.2 (M + NH_4).

*5.1.5. General procedure for the synthesis of **12a** and **12b***

A mixture of **9a** (or **9b**) (1 mmol), 15 ml NaOH (1 mol/L) and 15 ml methanol was heated to 60 °C for 3.5 h. After completion of the reaction as monitored by TLC, the pH of the mixture was regulated to 3–5 by hydrochloric acid (1 mol/L). The solid obtained (**12a** or **12b**) was filtered.

*5.1.5.1. (E)-2-(3-benzyl-4-(4-hydroxybenzylidene)-2,5-dioxoimidazolidin-1-yl)acetic acid(**12a**).* A yellow solid with the following characteristics: 68.32% yield; m.p. 192.5–193.4 °C; ^{1}H NMR (DMSO-d_6, 400 MHz): δ 13.234 (1H, s, COOH); 9.894 (1H, s, Ar–OH); 7.823 (2H, d, J = 8.72 Hz, Ar–H); 7.362–7.276 (5H, m, Ar–H); 6.737 (2H, d, J = 8.72 Hz, Ar–H); 6.485 (1H, s, =CH); 4.978 (2H, s, N–CH_2); 4.268 (2H, s, N–CH_2); MS (m/z): 370.2 (M + NH_4).

*5.1.5.2. (E)-4-((3-benzyl-4-(4-hydroxybenzylidene)-2,5-dioxoimidazolidin-1-yl)methyl)benzoic acid(**12b**).* A yellow solid with the following characteristics: 62.37% yield; m.p. 197.9–198.7 °C; ^{1}H NMR (DMSO-d_6, 400 MHz): δ 12.833 (1H, s, COOH); δ 10.022 (1H, s, Ar–OH); 7.932 (2H, d, J = 8.00 Hz, Ar–H); 7.835 (2H, d, J = 8.40 Hz, Ar–H); 7.755 (2H, d, J = 8.00 Hz, Ar–H); 7.356–7.465 (5H, m, Ar–H); 6.731 (2H, d, J = 8.40 Hz, Ar–H); 6.653 (1H, s, =CH); 4.970 (2H, s, N–CH_2); 4.808 (2H, s, N–CH_2); MS (m/z): 446.1 (M + NH_4).

*5.1.6. General procedure for the synthesis of **13a–13c***

12a (or **12b**) (1 mmol), methyl 4-(bromomethyl) benzoate (or methyl bromoacetate) (4 mmol) and K_2CO_3 (4 mmol) were dissolved in 50 ml DMF. The mixture was stirred at 75 °C for 3 h, and TLC examination showed the reaction was complete. Then, the mixture was concentrated, extracted by distilled water, ethyl acetate and saturated brine, and dried over anhydrous $MgSO_4$. The resulting residue was purified by column chromatography with petroleum ether: ethyl acetate = 8:1–4:1 to give **13a** or **13b** (or **13c**).

*5.1.6.1. (E)-Methyl 4-((4-((3-benzyl-1-(2-((4-(methoxycarbonyl) benzyl)oxy)-2-oxoethyl)-2,5-dioxoimidazolidin-4-ylidene)methyl) phenoxy)methyl)benzoate(**13a**).* A pale yellow solid with the following characteristics: 59.21% yield; m.p. 179.8–180.6 °C; ^{1}H NMR (DMSO-d_6, 400 MHz): δ 7.778 (2H, t, J = 8.80 Hz, Ar–H); δ 7.777 (2H, t, J = 8.80 Hz, Ar–H); 7.476 (2H, d, J = 8.40 Hz, Ar–H); 7.410 (2H, d, J = 8.00 Hz, Ar–H); 7.410 (2H, d, J = 8.00 Hz, Ar–H); 7.260–7.332 (5H, m, Ar–H); 8.901 (2H, d, J = 9.20 Hz, Ar–H); 6.207 (1H, s, =CH); 5.264 (2H, s, N–CH_2); 5.130 (2H, s, CH_2); 4.952 (2H, s, N–CH_2); 4.497 (2H, s, CH_2); 3.922 (3H, s, OCH_3); 3.917 (3H, s, OCH_3); MS (m/z): 666.2 (M + NH_4).

*5.1.6.2. (E)-2-Methoxy-2-oxoethyl 2-(3-benzyl-4-(4-(2-methoxy-2-oxoethoxy)benzylidene)-2,5-dioxoimidazolidin-1-yl)acetate(**13b**).* A white solid with the following characteristics: 68.91% yield; m.p. 96.1–96.8 °C; ^{1}H NMR (DMSO-d_6, 400 MHz): δ 7.893 (2H, d, J = 8.40 Hz, Ar–H); 7.283–7.356 (5H, m, Ar–H); 6.933 (2H, d, J = 8.40 Hz, Ar–H); 6.578 (1H, s, =CH); 4.999 (2H, s, N–CH_2); 4.838 (2H, s, OCH_2); 4.834 (2H, s, OCH_2); 4.505 (2H, s, N–CH_2); 3.690 (3H, s, OCH_3); 3.682 (3H, s, OCH_3); MS (m/z): 514.2 (M + NH_4).

*5.1.6.3. (E)-2-Methoxy-2-oxoethyl 4-((3-benzyl-4-(4-(2-methoxy-2-oxoethoxy)benzylidene)-2,5-dioxoimidazolidin-1-yl)methyl)benzoate(**13c**).* A white solid with the following characteristics: 72.34% yield; m.p. 154.6–155.3 °C; ^{1}H NMR (DMSO-d_6, 400 MHz): δ 7.298 (2H, d, J = 6.00 Hz, Ar–H); 7.268 (2H, d, J = 7.80 Hz, Ar–H); 7.111 (2H, d, J = 8.00 Hz, Ar–H); 6.839–7.864 (5H, m, Ar–H); 6.578 (2H, d, J = 6.80 Hz, Ar–H); 6.187 (1H, s, =CH); 4.938 (2H, s, O–CH_2); 4.862 (2H, s, N–CH_2); 4.768 (2H, s, N–CH_2); 4.633 (2H, s, O–CH_2); 3.793 (3H, s, OCH_3); 3.785 (3H, s, OCH_3); MS (m/z): 590.1 (M + NH_4).

*5.1.7. General procedure for the synthesis of **10g***

According to the synthesis of **10a-10f**, a mixture of benzyl hydantoin (4 mmol), ethyl 2-bromoacetate (4 mmol) and K_2CO_3 (4 mmol) in 30 ml DMF was heated to 85 °C for 3 h to produce ethyl 2-(3-benzyl-2,5-dioxoimidazolidin-1-yl)acetate **(8c)**. Then, the compound **8c** was used to react with 4-hydroxybenzaldehyde to afford ethyl 2-(3-benzyl-4-(4-hydroxybenzylidene)-2,5-dioxoimidazolidin-1-yl)acetate **(9c),** which reacted with benzyl chloride to afford the target compound **10g**.

*5.1.7.1. (E)-Ethyl 2-(3-benzyl-4-(4-(benzyloxy)benzylidene)-2,5-dioxoimidazolidin-1-yl)acetate(**10g**).* A white solid with the following characteristics: 84.21% yield; m.p. 107.2–107.9 °C; ^{1}H NMR (DMSO-d_6, 400 MHz): δ 7.906 (2H, d, J = 8.80 Hz, Ar–H); 7.386–7.450 (5H, m, Ar–H); 7.282–7.335 (5H, m, Ar–H); 7.009 (2H, d, J = 8.8 0 Hz, Ar–H); 6.565 (1H, s, =CH); 5.133 (2H, s, N–CH_2); 4.994 (2H, s, O–CH_2); 4.384 (2H, s, N–CH_2); 4.173 (2H, q, J = 6.80 Hz, OCH_2–); 1.216 (3H, t, J = 7.20 Hz, –CH_3); MS (m/z): 488.3 (M + NH_4).

5.2. Biological assay

The PTP1B activity was assayed using pNPP (Para-Nitro Phenyl Phosphate) as the substrate in 96-well plate. pNPP can be hydrolyzed by PTP1B to give para-nitrophenol. Para-nitrophenol will convert into para-nitrophenolate (pNP), which is an intense yellow compound and can be measured with a spectrophotometer after stopping solution was added. The regents used in this biological assay were as follows: human recombinant PTP1B, expressed in E coli and purified by Ni-NTA affinity chromatography in our lab; buffer, consisting of 50 mM citrate (pH 6.0), 0.1 M NaCl, 1 mM EDTA and 1 mM dithiothreitol (DTT); substrate, 2 mM pNPP in buffer; stopping solution, 0.2 M sodium hydroxide. PTP1B and tested compounds with multifarious concentrations mixed in 50 μL buffer were added to each well of a 96-well plate. PTP1B was replaced by an equivalent volume of buffer in blank. After pre-incubation for 15 min at room temperature, 50 μL substrate was added and incubated at 37 °C for 30 min, then stopping the

reaction by adding 10 μL 0.2 M sodium hydroxide and chilled on ice quickly and the absorption of plate was measured at 405 nm against blank. The following relation was used: OD405 = ε·b·[pNP], the molar absorption coefficient of pNP was 17,800 M^{-1} cm^{-1}, b was the light path (cm), and [pNP] was the pNP concentration. IC_{50} values were calculated by analyzing the data using OriginPro 7.5 software.

5.3. 3D-QSAR model

5.3.1. Dataset

Table 1 listed the structures and biological data of imidazolidine-2,4-dione derivatives, which were used to construct 3D-QSAR (CoMFA and CoMSIA) [39,40] models. Selections of test set molecules were made by considering the fact that test set molecules represent biological and structural diversity of training set molecules. Besides, the molecules of test set represent 20% of training set, which is regarded as a good percentage to validate a molecular model [41–46]. Based on above principle, the dataset was divided into training set and test set comprising 32 and 7 compounds, respectively. For QSAR analysis, IC_{50} values were converted to pIC_{50} values according to the following equation:

$$pIC_{50} = -\log IC_{50}$$

5.3.2. Structural optimization and alignment

The CoMFA/CoMSIA studies were performed on a Dell computer workstation with the Linux operating system using the SYBYL-X 1.1.1 software package [47]. Energy minimizations were performed using Gasteiger-huckel charge and Tripos force field with a distance-dependent dielectric and the Powell conjugate gradient algorithm with convergence criterion of 0.05 kcal/mol [45]. Subsequently, all structures were aligned by the common substructure using "molecular alignment" [48,49] with the most active compound **5e** was chosen as a template molecule (Fig. 8).

5.3.3. CoMFA/CoMSIA interaction energy calculation

For aligned training set, CoMFA steric and electrostatic fields were calculated at each lattice point with grid spacing value of 2.0 Å in all Cartesian directions. A default sp^3 C probe atom with a Van-Der Waals radius of 1.52 Å and a charge of ±1.0 was used to generate Steric (Lennard-Jones 6–12 potential) field energies and Electrostatic (Coulombic potential) fields. The computed field energies were truncated to 30 kcal/mol for both Steric and Electrostatic fields. CoMSIA calculates steric, electrostatic, hydrophobic, hydrogen-bond donor and acceptor fields with the same lattice box and probe atom used for the CoMFA calculations. The attenuation factor α, which determines the steepness of the Gaussian function, was assigned a default value of 0.3, and an optimal value normally ranging from 0.2 to 0.4 [50–53].

5.3.4. Partial least squares (PLS) analysis

Partial least square was used to linearly correlate the CoMFA/CoMSIA fields to the bioactivity. Cross-validation was performed by the Leave-One-Out (LOO) procedure to determine the optimum number of components (ONC). Based on ONC, the non-cross-validation was performed to give the conventional correlation coefficients (r^2), standard error, and the F ratio. The predictive correlation coefficient (r^2_{pred}) was calculated using test set to further verify the predictive ability of the model.

5.4. Molecular docking

The Surflex-Dock [54–57] module in the SYBYL-X 1.1.1 molecular modeling package [47] was used to undertake molecular docking for all studied compounds with target. The 3D structure of PTP1B was taken from the Brookhaven Protein Databank (PDB code: 2QBQ). Firstly, the compounds were prepared via the ligand structure preparation module "sanitize", which involved filling valences, checking for correctness, standardizing, removing duplicates and producing only one molecule of input structure [58,59]. Then, the receptor PTP1B was prepared. The hydrogen and missing atoms were added, waters were removed and the energy was minimized to obtain the docking receptor [60]. Finally, Surflex-docking guided by protomol "Ligand mode" [61] was carried out. In this mode, the receptor binding pocket was defined by the coordinate space of the extracted co-crystallized ligand [62–64]. The threshold and bloat parameters with value of 0.50 and 0 Å were established to determine the extent of the binding pocket [65]. During the docking process, the ligand generated various conformations to fit the receptor, in which the top 20 were displayed in the result list according to their docking score [66]. The ligand conformation with the highest total score was analyzed for the interactions with receptor PTP1B.

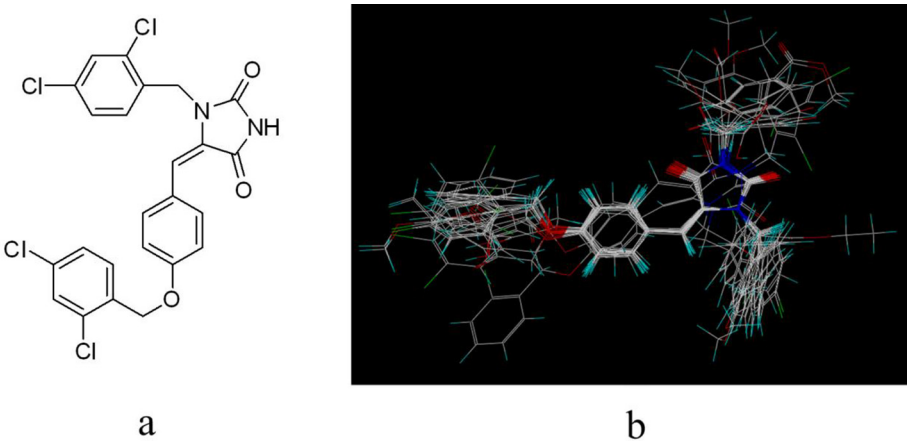

Fig. 8. (a) Structure of template molecule **5e** used for molecular alignment of imidazolidine-2,4-dione derivatives. (b) Molecular alignment.

Acknowledgments

This study was supported by the National Natural Science Foundation of China (Grant No. 81273361 and 21202120), China Postdoctoral Science Foundation funded project (2014T70222).

References

[1] J.M. Chehade, A.D. Mooradian, A rational approach to drug therapy of type 2 diabetes mellitus, Drugs 60 (2000) 95–113.
[2] C.R. Chittleborough, J.F. Grant, P.J. Phillips, A.W. Taylor, The increasing prevalence of diabetes in South Australia: the relationship with population ageing and obesity, Public Health 121 (2007) 92–99.
[3] L. Blonde, Current challenges in diabetes management, Clin. Cornerstone 7 (Suppl. 3) (2005) S6–S17.
[4] S.J. Patankar, P.C. Jurs, Classification of inhibitors of protein tyrosine phosphatase 1B using molecular structure based descriptors, J. Chem. Inf. Comput. Sci. 43 (2003) 885–899.
[5] J. Tobin, S. Tam, Recent advances in the development of small molecule inhibitors of PTP1B for the treatment of insulin resistance and type 2 diabetes, Curr. Opin. Drug Discov. Dev. 5 (2002) 500–512.
[6] G. Liu, J.M. Trevillyan, Protein tyrosine phosphatase 1B as a target for the treatment of impaired glucose tolerance and type II diabetes, Curr. Opin. Investig. Drugs 3 (2002) 1608–1616.
[7] T.O. Johnson, J. Ermolieff, M.R. Jirousek, Protein tyrosine phosphatase 1B inhibitors for diabetes, Nat. Rev. Drug Discov. 1 (2002) 696–709.
[8] T. Hunter, Protein kinases and phosphatases: the yin and yang of protein phosphorylation and signaling, Cell 80 (1995) 225–236.
[9] J.L. Evans, B. Jallal, Protein tyrosine phosphatases: their role in insulin action and potential as drug targets, Expert Opin. Invest. Drugs 8 (1999) 139–160.
[10] A. Ostman, F.D. Bohmer, Regulation of receptor tyrosine kinase signaling by protein tyrosine phosphatases, Trends Cell Biol. 11 (2001) 258–266.
[11] M. Elchebly, P. Payette, E. Michaliszyn, W. Cromlish, S. Collins, A.L. Loy, D. Normandin, A. Cheng, J. Himms-Hagen, C.-C. Chan, Increased insulin sensitivity and obesity resistance in mice lacking the protein tyrosine phosphatase-1B gene, Science 283 (1999) 1544–1548.
[12] L.D. Klaman, O. Boss, O.D. Peroni, J.K. Kim, J.L. Martino, J.M. Zabolotny, N. Moghal, M. Lubkin, Y.B. Kim, A.H. Sharpe, A. Stricker-Krongrad, G.I. Shulman, B.G. Neel, B.B. Kahn, Increased energy expenditure, decreased adiposity, and tissue-specific insulin sensitivity in protein-tyrosine phosphatase 1B-deficient mice, Mol. Cell. Biol. 20 (2000) 5479–5489.
[13] G. Liu, Technology evaluation: ISIS-113715, Isis, Curr. Opin. Mol. Ther. 6 (2004) 331–336.
[14] S. Koren, I.G. Fantus, Inhibition of the protein tyrosine phosphatase PTP1B: potential therapy for obesity, insulin resistance and type-2 diabetes mellitus, Best Pract. Res. Clin. Endocrinol. Metab. 21 (2007) 621–640.
[15] S. Lee, Q. Wang, Recent development of small molecular specific inhibitor of protein tyrosine phosphatase 1B, Med. Res. Rev. 27 (2007) 553–573.
[16] S. Zhang, Z.-Y. Zhang, PTP1B as a drug target: recent developments in PTP1B inhibitor discovery, Drug Discov. Today 12 (2007) 373–381.
[17] Z.-Q. Liu, T. Liu, C. Chen, M.-Y. Li, Z.-Y. Wang, R.-s. Chen, G.-x. Wei, X.-y. Wang, D.-Q. Luo, Fumosorinone, a novel PTP1B inhibitor, activates insulin signaling in insulin-resistance HepG2 cells and shows anti-diabetic effect in diabetic KKAy mice, Toxicol. Appl. Pharmacol.
[18] H.B. He, L.X. Gao, Q.F. Deng, W.P. Ma, C.L. Tang, W.W. Qiu, J. Tang, J.Y. Li, J. Li, F. Yang, Synthesis and biological evaluation of 4,4-dimethyl lithocholic acid derivatives as novel inhibitors of protein tyrosine phosphatase 1B, Bioorg. Med. Chem. Lett. 22 (2012) 7237–7242.
[19] M.V. Reddy, C. Ghadiyaram, S.K. Panigrahi, S. Hosahalli, L.N. Mangamoori, Diphenylether derivative as selective inhibitor of protein tyrosine phosphatase 1B (PTP1B) over t-cell protein tyrosine phosphatase (TCPTP) identified through virtual screening, Mini Rev. Med. Chem. 13 (2013) 1602–1606.
[20] A. Tsuchiya, T. Kanno, T. Nishizaki, Stearic acid serves as a potent inhibitor of protein tyrosine phosphatase 1B, Cell. Physiol. Biochem. 32 (2013) 1451–1459.
[21] M. Ito, S. Fukuda, S. Sakata, H. Morinaga, T. Ohta, Pharmacological effects of JTT-551, a novel protein tyrosine phosphatase 1B inhibitor, in diet-induced obesity mice, J. Diabetes Res. 2014 (2014) 680348.
[22] Y. Li, Y. Yu, K. Jin, L. Gao, T. Luo, L. Sheng, X. Shao, J. Li, Synthesis and biological evaluation of novel thiadiazole amides as potent Cdc25B and PTP1B inhibitors, Bioorg. Med. Chem. Lett. 24 (2014) 4125–4128.
[23] A. Maeda, K. Kai, M. Ishii, T. Ishii, M. Akagawa, Safranal, a novel protein tyrosine phosphatase 1B inhibitor, activates insulin signaling in C2C12 myotubes and improves glucose tolerance in diabetic KK-Ay mice, Mol. Nutr. Food Res. 58 (2014) 1177–1189.
[24] Z. Qin, N.R. Pandey, X. Zhou, C.A. Stewart, A. Hari, H. Huang, A.F.R. Stewart, J.M. Brunel, H.-H. Chen, Functional properties of Claramine: a novel PTP1B inhibitor and insulin-mimetic compound, Biochem. Biophys. Res. Commun. 458 (2015) 21–27.
[25] R. Maccari, P. Paoli, R. Ottana, M. Jacomelli, R. Ciurleo, G. Manao, T. Steindl, T. Langer, M.G. Vigorita, G. Camici, 5-Arylidene-2,4-thiazolidinediones as inhibitors of protein tyrosine phosphatases, Bioorg. Med. Chem. 15 (2007) 5137–5149.
[26] R. Ottana, R. Maccari, R. Ciurleo, P. Paoli, M. Jacomelli, G. Manao, G. Camici, C. Laggner, T. Langer, 5-Arylidene-2-phenylimino-4-thiazolidinones as PTP1B and LMW-PTP inhibitors, Bioorg. Med. Chem. 17 (2009) 1928–1937.
[27] B.R. Bhattarai, B. Kafle, J.-S. Hwang, D. Khadka, S.-M. Lee, J.-S. Kang, S.W. Ham, I.-O. Han, H. Park, H. Cho, Thiazolidinedione derivatives as PTP1B inhibitors with antihyperglycemic and antiobesity effects, Bioorg. Med. Chem. Lett. 19 (2009) 6161–6165.
[28] M. Sarmiento, L. Wu, Y.F. Keng, L. Song, Z. Luo, Z. Huang, G.Z. Wu, A.K. Yuan, Z.Y. Zhang, Structure-based discovery of small molecule inhibitors targeted to protein tyrosine phosphatase 1B, J. Med. Chem. 43 (2000) 146–155.
[29] Y. Cheng, M. Zhou, C.-H. Tung, M. Ji, F. Zhang, Studies on two types of PTP1B inhibitors for the treatment of type 2 diabetes: hologram QSAR for OBA and BBB analogues, Bioorg. Med. Chem. Lett. 20 (2010) 3329–3337.
[30] M. Zhou, M. Ji, Molecular docking and 3D-QSAR on 2-(oxalylamino) benzoic acid and its analogues as protein tyrosine phosphatase 1B inhibitors, Bioorg. Med. Chem. Lett. 15 (2005) 5521–5525.
[31] P.C. Nair, M.E. Sobhia, CoMFA based de novo design of pyridazine analogs as PTP1B inhibitors, J. Mol. Graph. Model. 26 (2007) 117–123.
[32] S. Thareja, S. Aggarwal, T.R. Bhardwaj, M. Kumar, Self-organizing molecular field analysis of 2,4-thiazolidinediones: a 3D-QSAR model for the development of human PTP1B inhibitors, Eur. J. Med. Chem. 45 (2010) 2537–2546.
[33] A.O. Ajala, C.O. Okoro, CoMFA and CoMSIA studies on fluorinated hexahydropyrimidine derivatives, Bioorg. Med. Chem. Lett. 21 (2011) 7392–7398.
[34] M.A. Khanfar, D.T. Youssef, K.A. El Sayed, 3D-QSAR studies of latrunculin-based actin polymerization inhibitors using CoMFA and CoMSIA approaches, Eur. J. Med. Chem. 45 (2010) 3662–3668.
[35] R.B. Huang, Q.S. Du, C.H. Wang, K.C. Chou, An in-depth analysis of the biological functional studies based on the NMR M2 channel structure of influenza A virus, Biochem. Biophys. Res. Commun. 377 (2008) 1243–1247.
[36] S.Q. Wang, Q.S. Du, R.B. Huang, D.W. Zhang, K.C. Chou, Insights from investigating the interaction of oseltamivir (Tamiflu) with neuraminidase of the 2009 H1N1 swine flu virus, Biochem. Biophys. Res. Commun. 386 (2009) 432–436.
[37] Q.H. Liao, Q.Z. Gao, J. Wei, K.C. Chou, Docking and molecular dynamics study on the inhibitory activity of novel inhibitors on epidermal growth factor receptor (EGFR), Med. Chem. 7 (2011) 24–31.
[38] D.P. Wilson, Z.K. Wan, W.X. Xu, S.J. Kirincich, B.C. Follows, D. Joseph-McCarthy, K. Foreman, A. Moretto, J. Wu, M. Zhu, E. Binnun, Y.L. Zhang, M. Tam, D.V. Erbe, J. Tobin, X. Xu, L. Leung, A. Shilling, S.Y. Tam, T.S. Mansour, J. Lee, Structure-based optimization of protein tyrosine phosphatase 1B inhibitors: from the active site to the second phosphotyrosine binding site, J. Med. Chem. 50 (2007) 4681–4698.
[39] R.D. Cramer, D.E. Patterson, J.D. Bunce, Comparative molecular field analysis (CoMFA). 1. Effect of shape on binding of steroids to carrier proteins, J. Am. Chem. Soc. 110 (1988) 5959–5967.
[40] G. Klebe, U. Abraham, T. Mietzner, Molecular similarity indices in a comparative analysis (CoMSIA) of drug molecules to correlate and predict their biological activity, J. Med. Chem. 37 (1994) 4130–4146.
[41] E. Cichero, S. Cesarini, P. Fossa, A. Spallarossa, L. Mosti, Thiocarbamates as non-nucleoside HIV-1 reverse transcriptase inhibitors: docking-based CoMFA and CoMSIA analyses, Eur. J. Med. Chem. 44 (2009) 2059–2070.
[42] S.Y. Liao, L. Qian, T.F. Miao, H.L. Lu, K.C. Zheng, CoMFA and docking studies of 2-phenylindole derivatives with anticancer activity, Eur. J. Med. Chem. 44 (2009) 2822–2827.
[43] J. Perez-Villanueva, J.L. Medina-Franco, T.R. Caulfield, A. Hernandez-Campos, F. Hernandez-Luis, L. Yepez-Mulia, R. Castillo, Comparative molecular field analysis (CoMFA) and comparative molecular similarity indices analysis (CoMSIA) of some benzimidazole derivatives with trichomonicidal activity, Eur. J. Med. Chem. 46 (2011) 3499–3508.
[44] C. Gueto, J. Torres, R. Vivas-Reyes, CoMFA, LeapFrog and blind docking studies on sulfonanilide derivatives acting as selective aromatase expression regulators, Eur. J. Med. Chem. 44 (2009) 3445–3451.
[45] S. Pirhadi, J.B. Ghasemi, 3D-QSAR analysis of human immunodeficiency virus entry-1 inhibitors by CoMFA and CoMSIA, Eur. J. Med. Chem. 45 (2010) 4897–4903.
[46] S.R. Patel, R. Gangwal, A.T. Sangamwar, R. Jain, Synthesis, biological evaluation and 3D-QSAR study of hydrazide, semicarbazide and thiosemicarbazide derivatives of 4-(adamantan-1-yl)quinoline as anti-tuberculosis agents, Eur. J. Med. Chem. 85 (2014) 255–267.
[47] R.W. Homer, J. Swanson, R.J. Jilek, T. Hurst, R.D. Clark, SYBYL line notation (SLN): a single notation to represent chemical structures, queries, reactions, and virtual libraries, J. Chem. Inf. Model. 48 (2008) 2294–2307.
[48] P. Aparoy, G.K. Suresh, K. Kumar Reddy, P. Reddanna, CoMFA and CoMSIA studies on 5-hydroxyindole-3-carboxylate derivatives as 5-lipoxygenase inhibitors: generation of homology model and docking studies, Bioorg. Med. Chem. Lett. 21 (2011) 456–462.
[49] P. Lu, X. Wei, R. Zhang, CoMFA and CoMSIA studies on HIV-1 attachment inhibitors, Eur. J. Med. Chem. 45 (2010) 1792–1798.
[50] K.C. Chou, D.Q. Wei, W.Z. Zhong, Binding mechanism of coronavirus main proteinase with ligands and its implication to drug design against SARS, Biochem. Biophys. Res. Commun. 308 (2003) 148–151.
[51] Q. Du, S. Wang, D. Wei, S. Sirois, K.C. Chou, Molecular modeling and chemical modification for finding peptide inhibitor against severe acute respiratory syndrome coronavirus main proteinase, Anal. Biochem. 337 (2005) 262–270.

[52] Q.S. Du, R.B. Huang, C.H. Wang, X.M. Li, K.C. Chou, Energetic analysis of the two controversial drug binding sites of the M2 proton channel in influenza A virus, J. Theor. Biol. 259 (2009) 159–164.
[53] H. Wei, C.H. Wang, Q.S. Du, J. Meng, K.C. Chou, Investigation into adamantane-based M2 inhibitors with FB-QSAR, Med. Chem. 5 (2009) 305–317.
[54] R. Spitzer, A.N. Jain, Surflex-Dock: docking benchmarks and real-world application, J. Comput. Aided Mol. Des. 26 (2012) 687–699.
[55] A.N. Jain, Surflex-Dock 2.1: robust performance from ligand energetic modeling, ring flexibility, and knowledge-based search, J. Comput. Aided Mol. Des. 21 (2007) 281–306.
[56] M.A. Miteva, W.H. Lee, M.O. Montes, B.O. Villoutreix, Fast structure-based virtual ligand screening combining FRED, DOCK, and Surflex, J. Med. Chem. 48 (2005) 6012–6022.
[57] A.N. Jain, Surflex: fully automatic flexible molecular docking using a molecular similarity-based search engine, J. Med. Chem. 46 (2003) 499–511.
[58] S.S. Rozenel, J.B. Kerr, J. Arnold, Metal complexes of Co, Ni and Cu with the pincer ligand HN(CH2CH2P(i)Pr2)2: preparation, characterization and electrochemistry, Dalton Trans. 40 (2011) 10397–10405.
[59] G.M. Sastry, M. Adzhigirey, T. Day, R. Annabhimoju, W. Sherman, Protein and ligand preparation: parameters, protocols, and influence on virtual screening enrichments, J. Comput. Aided Mol. Des. 27 (2013) 221–234.
[60] J. Xu, Y.F. Ma, W.S. Liu, Y. Tang, M.Y. Tan, Preparation, crystal structures and luminescent properties of terbium and europium complexes with a new amino-alkenone type ligand, J. Fluoresc. 21 (2011) 35–42.
[61] J. Ruppert, W. Welch, A.N. Jain, Automatic identification and representation of protein binding sites for molecular docking, Protein Sci. 6 (1997) 524–533.
[62] J. Zhang, C.H. Luan, K.C. Chou, G.V. Johnson, Identification of the N-terminal functional domains of Cdk5 by molecular truncation and computer modeling, Proteins 48 (2002) 447–453.
[63] J.F. Wang, D.Q. Wei, L. Li, S.Y. Zheng, Y.X. Li, K.C. Chou, 3D structure modeling of cytochrome P450 2C19 and its implication for personalized drug design, Biochem. Biophys. Res. Commun. 355 (2007) 513–519.
[64] R.M. Pielak, J.R. Schnell, J.J. Chou, Mechanism of drug inhibition and drug resistance of influenza A M2 channel, Proc. Natl. Acad. Sci. U. S. A. 106 (2009) 7379–7384.
[65] M. Lape, C. Elam, S. Paula, Comparison of current docking tools for the simulation of inhibitor binding by the transmembrane domain of the sarco/endoplasmic reticulum calcium ATPase, Biophys. Chem. 150 (2010) 88–97.
[66] R.D. Clark, A. Strizhev, J.M. Leonard, J.F. Blake, J.B. Matthew, Consensus scoring for ligand/protein interactions, J. Mol. Graph. Model. 20 (2002) 281–295.